**Natural Hazards
and Earth
System Sciences**

Submarine mass wasting and associated tsunami risk offshore western Thailand, Andaman Sea, Indian Ocean

J. M. Schwab[1], **S. Krastel**[1], **M. Grün**[1], **F. Gross**[1], **P. Pananont**[2], **P. Jintasaeranee**[3], **S. Bunsomboonsakul**[4], **W. Weinrebe**[1], **and D. Winkelmann**[1]

[1]GEOMAR | Helmholtz Centre for Ocean Research Kiel, Germany
[2]Department of Earth Sciences, Faculty of Science, Kasetsart University, Bangkok, Thailand
[3]Department of Aquatic Science, Burapha University, Chonburi, Thailand
[4]Thailand Southeast Asia START Regional Center, Chulalongkorn University, Bangkok, Thailand

Correspondence to: J. M. Schwab (jschwab@geomar.de)

Abstract. 2-D seismic data from the top and the western slope of Mergui Ridge in water depths between 300 and 2200 m off the Thai west coast have been investigated in order to identify mass transport deposits (MTDs) and evaluate the tsunamigenic potential of submarine landslides in this outer shelf area. Based on our newly collected data, 17 mass transport deposits have been identified. Minimum volumes of individual MTDs range between 0.3 km^3 and 14 km^3. Landslide deposits have been identified in three different settings: (i) stacked MTDs within disturbed and faulted basin sediments at the transition of the East Andaman Basin to the Mergui Ridge; (ii) MTDs within a pile of drift sediments at the basin-ridge transition; and (iii) MTDs near the edge of/on top of Mergui Ridge in relatively shallow water depths (< 1000 m). Our data indicate that the Mergui Ridge slope area seems to have been generally unstable with repeated occurrence of slide events. We find that the most likely causes for slope instabilities may be the presence of unstable drift sediments, excess pore pressure, and active tectonics. Most MTDs are located in large water depths (> 1000 m) and/or comprise small volumes suggesting a small tsunami potential. Moreover, the recurrence rates of failure events seem to be low. Some MTDs with tsunami potential, however, have been identified on top of Mergui Ridge. Mass-wasting events that may occur in the future at similar locations may trigger tsunamis if they comprise sufficient volumes. Landslide tsunamis, emerging from slope failures in the working area and affecting western Thailand coastal areas therefore cannot be excluded, though the probability is very small compared to the probability of earthquake-triggered tsunamis, arising from the Sunda Trench.

1 Introduction

The extremely catastrophic tsunamis of December 2004 in the SE Indian Ocean and March 2011 in Japan, as well as many other incidents (NGDC/WDC Global Tsunami Event Database, 2012), show that tsunamis pose a major threat to low-lying coastal areas. Ocean-wide tsunamis are predominantly triggered by earthquakes, but submarine landslides are also known for their potential to trigger regional tsunamis of significant wave heights (Ward, 2001; Harbitz et al., 2006). A well-studied prehistoric example of a landslide-triggered tsunami is the Storegga Slide offshore Norway (Jansen et al., 1987; Dawson et al., 1988; Bondevik et al., 1997, 2005). Tsunami deposits associated with the Storegga Slide were reported from Iceland, Norway, Scotland and the Shetland Islands with run-up heights exceeding 20 m in places (Bondevik et al., 2003). Moreover, several recent examples for locally destructive tsunami hazards were associated with submarine landslides, such as the Grand Banks tsunami (1929, Canada) that killed 28 people (Hasegawa and Kanamori, 1987; Piper et al., 1999; Fine et al., 2005), a tsunami at Skagway Harbor (1994, Alaska) with one casualty (Kulikov et al., 1996) and the Sissano or Aitape tsunami (1998, Papua New Guinea) causing about 2000 fatalities (Tappin, 1999; Tappin et al., 2001; Matsumoto and Tappin, 2003). Extensive research and modeling of landslide tsunami generation has been undertaken (Ward, 2001; Harbitz et al., 2006; Grilli et al., 2009; Weiss et al., 2009). However, early warning of landslide tsunami hazards is difficult due to the fact that seismological (Lomax et al., 2007) or GPS (Blewitt et al., 2006; Sobolev et al., 2007) techniques,

applicable to earthquake induced tsunamis, are not useful to detect landslide-generated tsunamis due to the comparably small amount of seismic energy release and long-period-signal of submarine landslides (Brune et al., 2009, 2010). Moreover, the time lag between sediment failure and tsunami arrival at the coast in the near field of a submarine landslide might be too small to forewarn and evacuate endangered regions (Biscontin et al., 2004).

It is therefore important to gain thorough knowledge on current stability of the continental slope for individual areas, in order to estimate frequencies and dimensions of failures and rate probability of future failures. This in turn can be used to assess tsunami risk and preparedness for corresponding coastal areas, such as the Thai Andaman Sea coast. The vicinity of this coast to the seismically highly active Sunda Trench (NGDC, Global Significant Earthquake Database, 2012) makes the area vulnerable to tsunamis. The geological record reveals recurrent tsunami events of destructive dimensions that struck the Thai west coast (Jankaew et al., 2008; Fujino et al., 2009). A potentially unstable continental slope off the Thai coast may pose an additional risk from submarine landslides, whether co-seismically triggered or triggered by other factors, provided that these failures would be of tsunamigenic dimensions. Assessing this risk is the central task of the MASS-project (Morphodynamics and Slope Stability of the Andaman Sea Shelf Break) in the frame of the Thai-German cooperation TRIAS (Tracing Tsunami impacts on- and offshore in the Andaman Sea Region).

Bathymetric and sub-bottom profiler data were obtained during the first project phases MASS I and MASS II. Jintasaeranee et al. (2012) identified possible slumping areas, though these landslides are considered to be too small for having triggered a significant tsunami in the recent past. Jintasaeranee et al. (2012), however, did not investigate older slope failures. New seismic data were collected during the MASS III research cruise in January 2011. These data are used in this study to trace landslide-related features in the subsurface in order to (1) identify areas that show indications of previous slope failure, (2) estimate volumes/dimensions of slides, (3) determine pre-conditioning and trigger mechanisms, and (4) assess the tsunamigenic potential of the detected landslides. The terms "landslide" and/or "mass transport deposit (MTD)" are used in this paper in a broad sense, denoting all types of gravitational mass wasting products, irrespective of the process.

2 Regional setting

The study area is situated at the western outer Sunda shelf in the southeastern part of the Andaman Sea backarc-basin, about 250 km off Phuket (Fig. 1). A basement high, the Mergui Ridge, forms the outer shelf break, where water depths increase from 300 to 2200 m in the working area. The Mergui Ridge separates two adjacent basins, the East Andaman
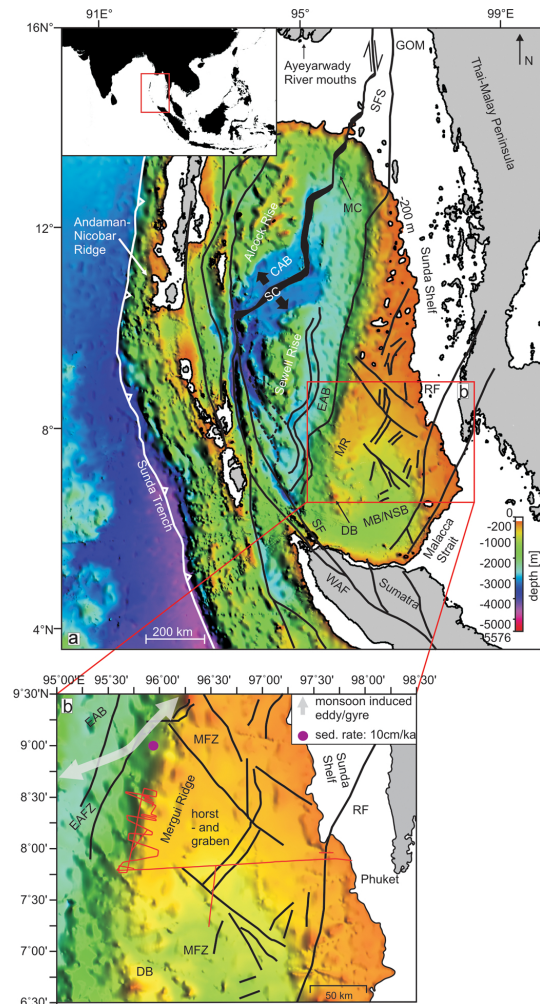
Fig. 1. (a) Bathymetric map and structural framework of the Andaman Sea area. The structural elements are modified from Curray (2005). Black continuous lines mark fault traces of the main fault systems: SFS: Sagaing Fault System; WAF: West Andaman Fault; RF: Ranong Fault; SF: Sumatra Fault System; GOM: Gulf of Martaban; MC: Martaban Canyon; SC: Modern spreading centre; CAB: Central Andaman Basin; EAB: East Andaman Basin; MR: Mergui Ridge; MB/NSB: Mergui Basin/North Sumatra Basin; DB: Dreadnought Bank. The bathymetry has been reproduced from GEBCO. (b) Close-up of the working area, situated in the western flank of Mergui Ridge. The red lines mark seismic lines of MASS III cruise. The black lines denote fault systems, modified after Curray (2005), Morley et al. (2011) and Polachan (1988). MFZ: Mergui Fault Zone (modified after Curray, 2005 and Morley et al., 2011. EAFZ: East Andaman Fault Zone (from Polachan, 1988). DB: Dreadnought Bank. EAB: East Andaman Basin. The grey arrow shows the approximate position of a monsoonal gyre that induces currents in deeper parts of the water column (modified after Varkey et al., 1996). The purple dot shows the position of a sediment core discussed by Rodolfo (1969). The bathymetry has been reproduced from SRTM30_PLUS (Becker et al., 2009).

Basin in the west and the Mergui Basin in the east and southeast (Fig. 1). The East Andaman Basin and the Mergui Basin are elongated, approximately NNE–SSW trending, sediment filled sub-basins of the Andaman Sea, located southwest of the Central Andaman Basin (Fig. 1, Curray, 2005). They have been described as rift basins (Hall and Morley, 2004; Jha et al., 2010), like numerous other Cenozoic basins across Sundaland (Polachan et al., 1991; Morley et al., 2001; Morley, 2002; Hall and Morley, 2004; Doust and Noble, 2008) and accordingly comprise a sedimentation history that is linked to typical rift stages (Doust and Noble, 2007; Doust and Sumner, 2008; Jha et al., 2010). The formation of the East Andaman Basin and the Mergui Basin results from backarc-related extensional tectonics, active throughout the area (Chakraborty and Khan, 2009; Curray, 2005). For the development of the Andaman Sea basins multi-stage models have been suggested (Kamesh Raju et al., 2004; Curray, 2005; Kamesh Raju, 2005; Chakraborty and Khan, 2009). The area of rifting moved from the Mergui Basin over the East Andaman Basin to its current position (Fig. 1) during Oligocene to Pliocene, due to increasingly oblique plate motions and changing convergence rates of Indian and Sundaland plates (Curray, 2005). In the Central Andaman Basin active sea floor spreading has occured since 4 Ma (Kamesh Raju et al., 2004; Kamesh Raju, 2005; Khan and Chakraborty, 2009). This modern spreading center links a group of N–S striking dextral strike-slip faults (Sagaing Fault, West Andaman Fault and Sumatra Fault, Fig. 1a). This system is described to accommodate the oblique convergence of the Indian and Sundaland plates (Michel et al., 2001; Nielsen et al., 2004a; Curray, 2005; Socquet et al., 2006; Chakraborty and Khan, 2009).

The East Andaman Basin has been influenced by extensional and also strike-slip faulting. Kishore et al. (2010) described NE–SW trending extensional faults, truncated by N–S trending strike slip faults. W-NW facing listric block faulting at the western flank of Mergui Ridge was reported by Curray (2005). The general trend of main strike-slip faults in the East Andaman Basin area is N–S to NE–SW (Morley et al., 2011). The East Andaman Basin is bounded towards the Mergui Basin by the East Andaman Fault Zone (EAFZ, Fig. 1b), interpreted as a branch of the Sagaing Fault System (Polachan and Racey, 1994; Jha et al., 2010). North of the working area, the NW–SE trending strike-slip Mergui Fault is cutting across Mergui Ridge (Fig. 1b). Recent reactivation at this fault has been observed (Polachan and Racey, 1994).

The establishment of the Pliocene spreading center has been given as a reason for thermal subsidence of the area (Morley et al., 2011), which is still ongoing today (Lin et al., 2010). Moreover, right lateral movement along strike slip faults in the East Andaman Basin, such as the EAFZ, took place during the Late Miocene and caused subsidence and the development of mass wasting complexes west of the Mergui Ridge (Jha et al., 2010).

Today, the East Andaman Basin comprises a total sedimentary thickness of 4600 m (Curray, 2005). It is under a shallow- to deep- water regime since the Middle to Late Miocene (Curray, 2005; Jha, 2011) and post-rift sediments up to 2500 m thick have been deposited in this environment since the Middle Miocene (Jha et al., 2010). Presently, the main source for fine grained terrigenous sediment in the Andaman Sea is the Ayeyarwady-Salween river-system (Fig. 1a, Rodolfo, 1969; Colin et al., 1999). An enormous quantity of sediment is shed into the Andaman Sea (364 MT a^{-1}, Robinson et al., 2007), and a fraction of it reaches the deeper basins of the Andaman Sea via the Martaban Canyon (Fig. 1; Rao et al., 2005; Ramaswamy et al., 2004). An additional source of terrigenous input in the southern part of the Andaman Sea is the Malacca Strait (Fig. 1), delivering fine grained terrigenous detritus to the deeper parts of the Andaman Sea basins (Keller and Richards, 1967). Transport or deposition of terrigenous sediments on the outer shelf areas along Myanmar and the Thai-Malay peninsula (Sunda shelf, Fig. 1a), between the Ayeyarwady mouth and Mergui Ridge (Fig. 1a), is not important; these areas are described to be sediment starved (Rao et al., 2005; Ramaswamy et al., 2004; Panchang et al., 2008; Rodolfo, 1969), whereas the adjacent East Andaman Basin is one of the main depocenters in the Andaman Sea (Morley et al., 2011).

The recent hydrographic regime of the Andaman Sea is dominated by the Asian Monsoon, leading to seasonal reversal of upper ocean circulation directions (Wyrtki, 1961). During Northeast Monsoon (December–March) the circulation is cyclonic, whereas during Southwestern Monsoon (June–September) anticyclonic circulation prevails (Rao et al., 2005). Seasonal upwelling (Wirtky, 1961; Buranapratheprat et al., 2010) and lowered salinity in the surface waters due to freshwater discharge during SW Monsoon (Wirtky, 1961) are consequences of the monsoonal influence on the area. Circulation in greater water depths is affected as well. A steady, seasonal gyre is reported (Varkey et al., 1996) to be located slightly northwest of the working area (Fig. 1b). Lateral exchange with Indian Ocean water masses occurs at sills in the Andaman-Nicobar Ridge (Fig. 1, Wyrtki, 1961). They comprise maximum depths of around 1800 m. Below 1800 m exchange is restricted (Rodolfo, 1969; Dutta et al., 2007). However, a very uniform well mixed water mass is present in the deepest parts throughout the Andaman Sea (Varkey et al., 1996; Dutta et al., 2007). This implies vigorous vertical mixing (Dutta et al., 2007) with renewal times of about 6 yr (Okubo et al., 2004). Dutta et al. (2007) suggest that internal waves, creating turbulence over irregular topography, may be responsible for this mixing process. Large amplitude internal waves have indeed been reported to occur repeatedly in the Andaman Sea (Osborne and Burch, 1980; Nielsen et al., 2004b; Hyder et al., 2005; Vlasenko and Alpers, 2005). They are described to be created by tidal currents near the shallow sills of the Andaman and Nicobar island arc from where they travel eastward across the Andaman sea, propagating at

Table 1. Measured properties of identified MTDs in the working area.

MTD	Interpolated areal extent (km^2)	Maximum thickness of MTD (m)	Approx volume of MTD (km^3)	Depth of shallowest point from surface (m)
A1	70	56	1.3	1130
A2	27	36	0.3	1280
A3	33	55	0.8	1350
A4	69	166	3.0	1210
B1	24	91	1.0	1850
B2	10	46	0.3	1950
B3	43	135	3.0	1570
B4	53	150	3.4	1710
B5	27	125	1.5	2020
C1	23	76	0.7	1480
C2	46	89	2.6	1420
C3	45	90	2.1	1550
C4	32	62	1.0	1530
C5	22	72	1.0	1560
D1	40	75	0.9	880
D2	33	234	4.0	830
D3	585	62	14.0	640

density interfaces (Vlasenko and Alpers, 2005); over shallowing ground they may break and form turbulence (Osbourne and Burch, 1980; Hyder et al., 2005; Vlasenko and Stashuk, 2007). Scattering of an internal wave and creation of secondary internal waves has been reported from the southern tip of Mergui Ridge (Dreadnought Bank, Vlasenko and Alpers, 2005).

3 Dataset and methods

A total of 39 seismic reflection lines were collected at the transition Mergui Basin-Mergui Ridge-East Andaman Basin within the Thai exclusive economic zone in ESE–WNW and N–S directions during cruise MASS III from 11 January 2011 to 24 January 2011 (Fig. 1b). The total length of acquired seismic lines is about 630 km and the investigated area comprises approximately 5000 km^2. High resolution seismic reflection data were acquired using a micro GI-Gun (2 × 0.1 l) and a 150 m-long 96-channel digital Geometrics GeoEel streamer. The gun was operated at 120 bars and shot every 5 s resulting in a shotpoint distance of 10 m at vessel speeds of 4 knots. The main frequency used was 200 Hz. The streamer consisted of 12 sections with 8 channels each. The channel distance was 1.56 m. The signals were digitized at 4 kHz and converted into SEG-Y format for further processing.

Standard processing steps were performed with Vista Seismic Data Processing (GEDCO). After setup of the geometry, common midpoint sorting and normal moveout corrections were applied as well as bandpass frequency filtering for frequency contents of 25/50–600/1200 kHz, stacking and time-

migration (using a constant velocity of 1500 m s^{-1}). IHS Kingdom Suite was used for interpretation and volumetric calculations.

The bathymetry data set analysed in this study was obtained during previous cruises MASS I and MASS II in 2006 and 2007, using a portable Seabeam 1050 multibeam echo sounder. The system uses a frequency of 50 kHz, 126 individual beams and a swath width of up to 153° (Jintasaeranee et al., 2012). Resolution of the processed bathymetric grid is 50 m.

The general architecture of the background sedimentary units and the distributions and dimensions of mass transport deposits (MTDs) were deduced from the seismic dataset. MTDs were interpreted according to their external geometries and internal reflector characteristics. Examples of acoustic facies characteristics are given in Fig. 2. Lens- or wedge-shaped bodies showing a chaotic to transparent seismic facies were classified as MTDs. Precise measurements of volumes and areal extents of MTDs were not possible from our dataset, as spacing between profiles is relatively large, ranging between about 1 km and 7 km. Therefore, the geometries of the MTDs had to be interpolated over long distances of up to 7 km. An isopach grid was calculated, based on interpreted horizons of top and base for each MTD, using a constant sound velocity of 1500 m s^{-1}. Subsequently, volume and areal extent was deduced from the isopach grid. Values are summarized in Table 1. The values in Table 1, however, have to be regarded only as rough estimations due to the uncertainties mentioned above and due to the fact that the lateral boundaries of the MTDs are not present in our dataset, except for one MTD close to the sea floor, where boundaries
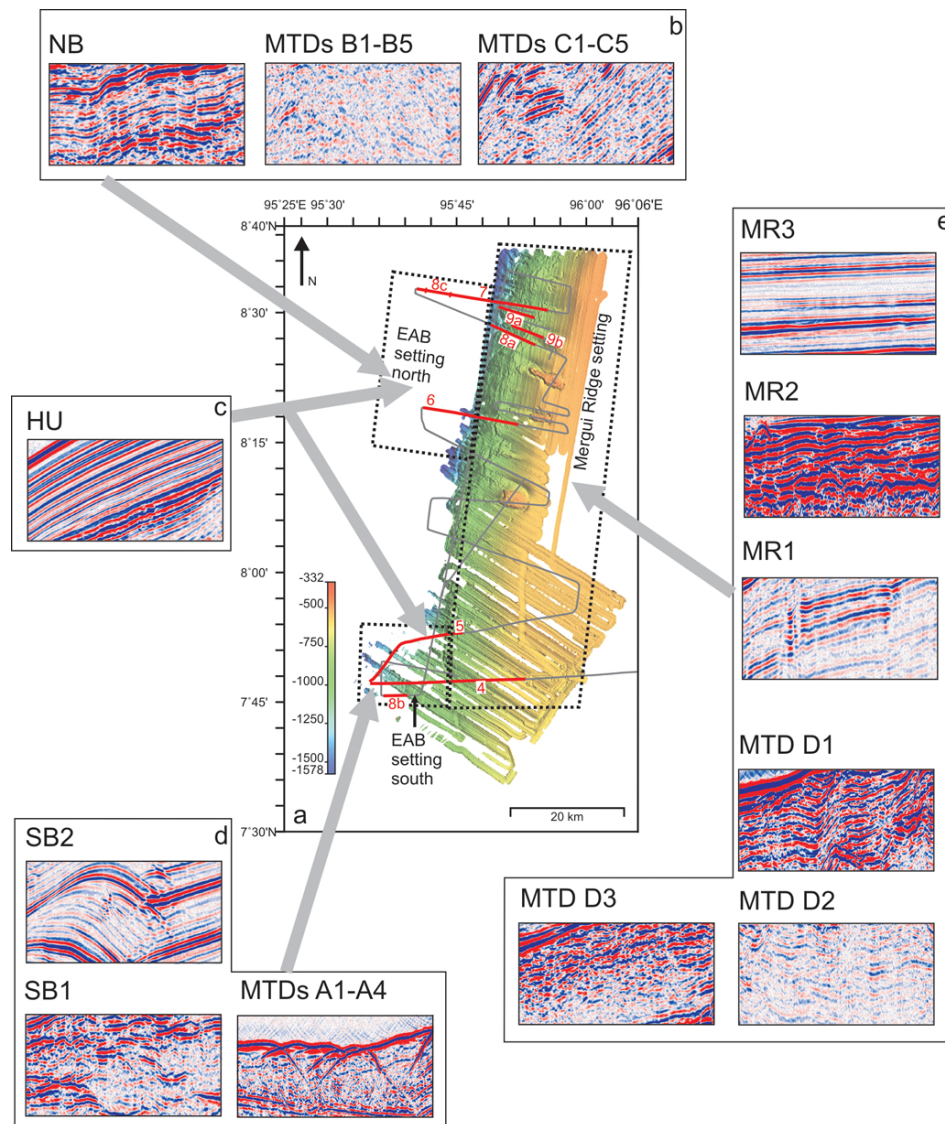
Fig. 2. (a) Bathymetric map of the working area modified after Jintasaeranee et al. (2012). The stippled black lines mark the three defined settings in the working area: Mergui Ridge, East Andaman Basin north and East Andaman Basin south. **(b)** Examples of the acoustic facies that were identified in the subsurface sediments of the northern working area, which are background sedimentary unit NB and MTDs B1–B5 and C1–C5. **(c)** Example of the acoustic facies of the surficial sedimentary unit HU identified throughout the East Andaman Basin area. **(d)** Examples of acoustic facies identified in the subsurface sediments of the southern working area, which are background sedimentary units SB1 and SB2 and MTDs A1–A4. **(e)** Examples of the acoustic facies identified in the Mergui Ridge setting, which are subsurface sedimentary units MR1 and MR2, surficial unit MR3 and MTDs D1–D3.

could be deduced from the bathymetry. Therefore, the values represent minimum estimates of individual MTDs, and actual volumes might be larger than mapped in this study. For a simple estimation of thickness of undisturbed sediment between the individual failure events, we calculated the thickness between the top and base horizon isopach grids of consecutive MTDs. For calculation of time intervals between the MTDs we used a sedimentation rate of $10\,\mathrm{cm\,ka^{-1}}$. This sedimentation rate was established by Rodolfo (1969) from a sediment core about 50 km north of our working area (Fig. 1b, approx-

imately $9°00'$ N, $95°57'$ E). The results of the calculations are given in Table 2.

4 Results

The investigated area is located at the transition from the Mergui Ridge/outer shelf area to the deep sea environment of the East Andaman Basin, and seismic profiles used in this study run across this basin-ridge transition (Figs. 1b, 2a and 3). Water depths are increasing from east (Mergui Ridge)
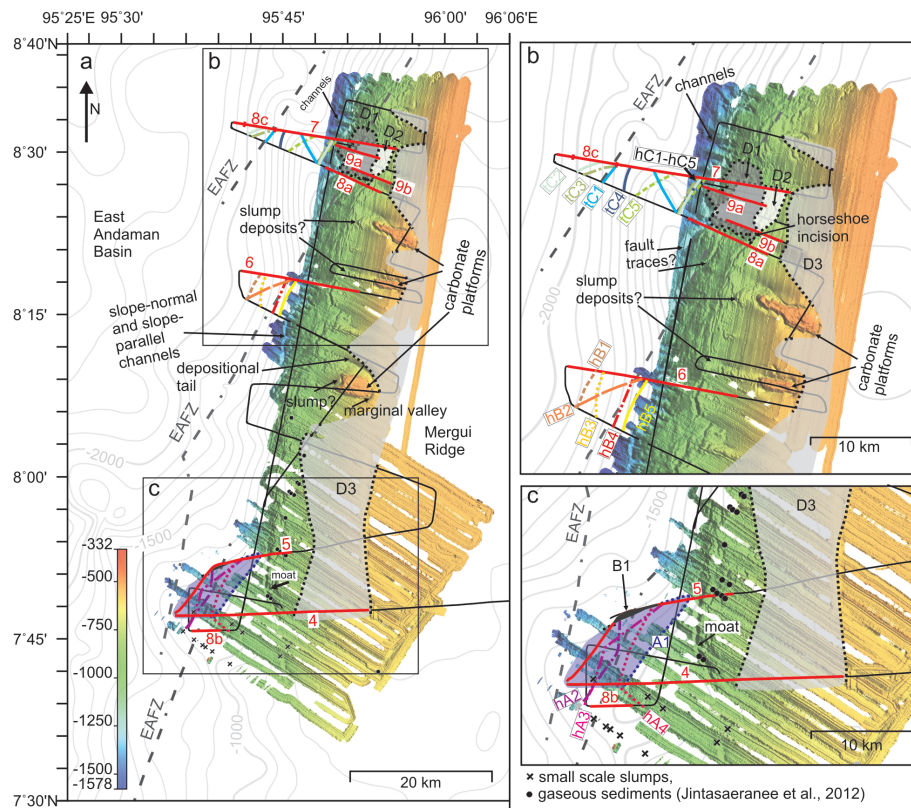
Fig. 3. (a) Bathymetric map of the working area (from Jintasearanee et al., 2012) with contour lines from SRTM30_PLUS (Becker et al., 2009). The interpretation of several morphological features, carbonate platforms, slump deposits, fault traces, as well as the positions of small scale slumps and gas-bearing sediment are taken from Jintasaeranee et al. (2012) as well. The black continuous lines show the cruise track and the red lines indicate the seismic profiles shown in this study. The grey shaded areas on the Mergui Ridge mark the areal extents of MTDs D1–D3, the black stippled lines show the slide margins where they were interpolated. The grey dotted lines indicate positions of branches of the EAFZ (from Polachan, 1988). **(b)** Close-up of the northern working area. The coloured dotted lines indicate heads (hB1–hB5 and hC1–hC5) and toes (tC1–tC5) of individual MTDs, as mapped from the seismic data. The grey shaded areas show the extents of the Mergui Ridge-MTDs D1–D3. **(c)** Close-up of the southern working area. The purple shaded area indicates the areal extent of MTD A1. The purple dotted line indicates the slide margins where they were interpolated. The dark grey block indicates the position of a potential in-situ block (B1, see also Fig. 5) or the slide margin north of A1. The coloured dotted lines denote the interpolated heads of MTDs A2–A4 (hA2–hA4).

to west (East Andaman Basin) from about 300 m to about 2200 m (Fig. 3). The western flank of Mergui Ridge forms the slope of the East Andaman Basin. Slope gradients of the basin–ridge transition are generally lower in the southern working area with values of about 1.5° (Figs. 4 and 5). Towards the north, slope angles at the edge of the Mergui Ridge are considerably higher, and reach, for example on Profile 14, values around 12° (Fig. 6). Downslope of the flank of the Mergui Ridge, the basin area is deepening towards the north (Fig. 3).

The bathymetric dataset reveals a very smooth seafloor on Mergui Ridge in the eastern part of the working area, except for three pronounced morphological highs that are pinching out from the flat top of Mergui Ridge (Fig. 3). In contrast, the sea-floor morphology is generally rough towards the western edge of the ridge. Several slope normal channels cut the edge of Mergui Ridge, and numerous elongated depressions run

approximately N–S to NNE–SSW (Fig. 3). Bathymetric features that have been examined in more detail by Jintasearanee et al. (2012) are marked on Fig. 3. Seismic data reveal a smooth relief further down the slope, where sediments of the East Andaman Basin are deposited (Figs. 6 and 7).

4.1 Background sedimentary units and their architecture

Based on the architecture of the basin-ridge transition, we differentiated three settings in the working area: (1) Mergui Ridge in the western part of the working area; (2) Basin sediments of the East Andaman Basin in the southern working area; (3) Basin sediments of the East Andaman Basin in the northern working area. The location of these three settings and an overview on the acoustic facies of the seismic units identified are given in Fig. 2.
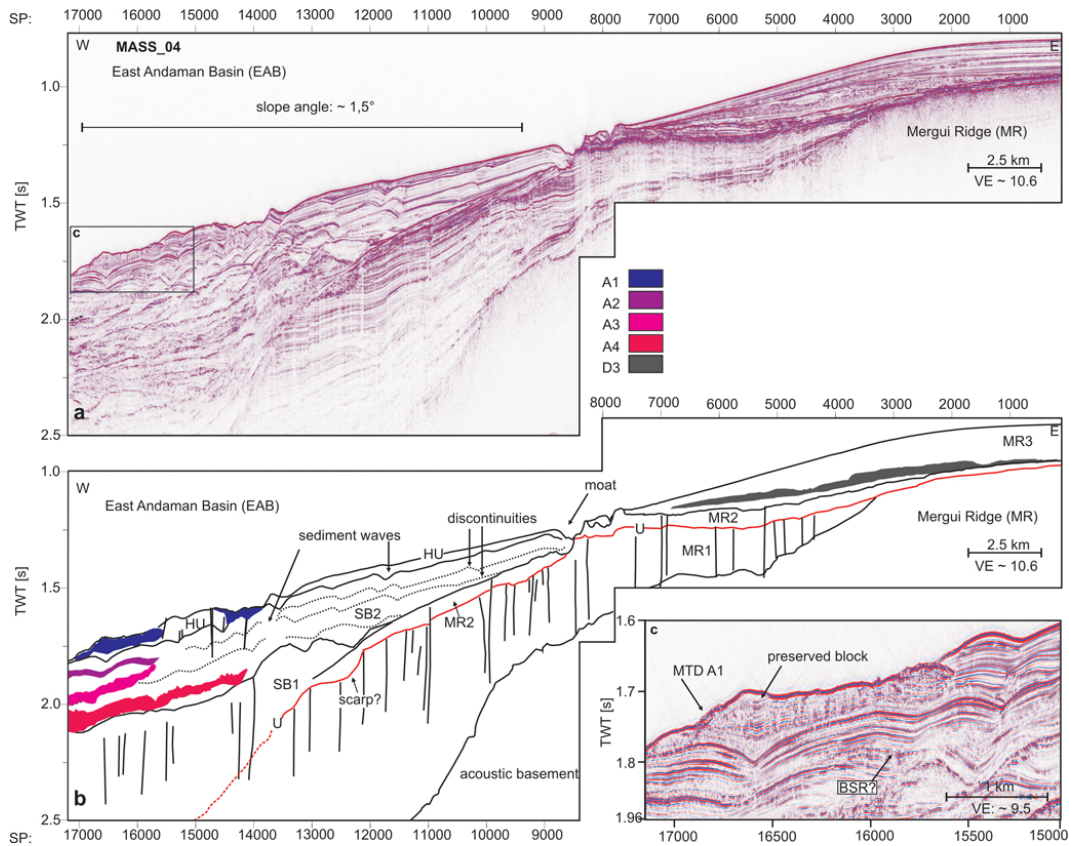
Fig. 4. (a) Seismic profile MASS_04 across the basin–ridge transition Mergui Ridge-East Andaman Basin in the southern working area. **(b)** Interpretation of the seismic profile showing the seismic units of Mergui Ridge in the east (MR1–MR3) and those of the southern East Andaman Basin area to the west. Faults are marked as black vertical lines. Black lines mark boundaries of seismic units. The black dashed lines mark the positions of possible discontinuities within SB2. The red line denotes the position of the unconformity U. The colored areas mark the position of the MTDs A1–A4. See Figs. 2 and 3 for location of profile. **(b)** Blowup of the superficial MTD A1, showing blocky structure of the deposit. The label BSR indicates the location of a potential bottom simulating reflector. See text for further explanations. See Figs. 2 and 3 for location of the profile.

Table 2. Calculated minimum time intervals between slide events, based on constant sedimentation rates of $10\,\mathrm{cm\,ka^{-1}}$ (from Rodolfo, 1969).

Interval between MTDs	Maximum thickness of undisturbed sediment between MTDs (m)	Calculated time interval (ka)
A1–A2	94	940
A2–A3	91	910
A3–A4	119	1190
B1–B2	39	390
B2–B3	22	220
B3–B4	96	960
B4–B5	147	1470
C1–C2	47	470
C2–C3	95	950
C3–C4	37	370
C4–C5	48	480

4.1.1 Mergui Ridge

The seismic units identified in the Mergui Ridge setting are laterally traceable on all profiles. We separated them into three seismic units: MR1 shows continuous parallel reflectors of variable amplitude (Fig. 2), and in the northern part towards its top a reflection pattern of transparent patches, alternating with chaotic high amplitude areas (Figs. 6 and 7); MR2 comprises high-amplitude, subparallel reflectors (Fig. 2); MR3 is characterized by parallel reflectors of variable amplitude with good lateral continuity (Fig. 2).

MR1 is overlying the acoustic basement at the western flank of Mergui Ridge (Fig. 4). It has a wedge-shaped geometry. The thinning of this unit towards the east and its reflector characteristics indicate deposition in a hemipelagic environment (Figs. 4 and 5). Deformation of MR1 is caused by numerous faults throughout the working area (Figs. 4–7). In the north, a section of MR1 sediments is exposed to the seafloor (Fig. 8a), indicating a recent erosive or non-depositional
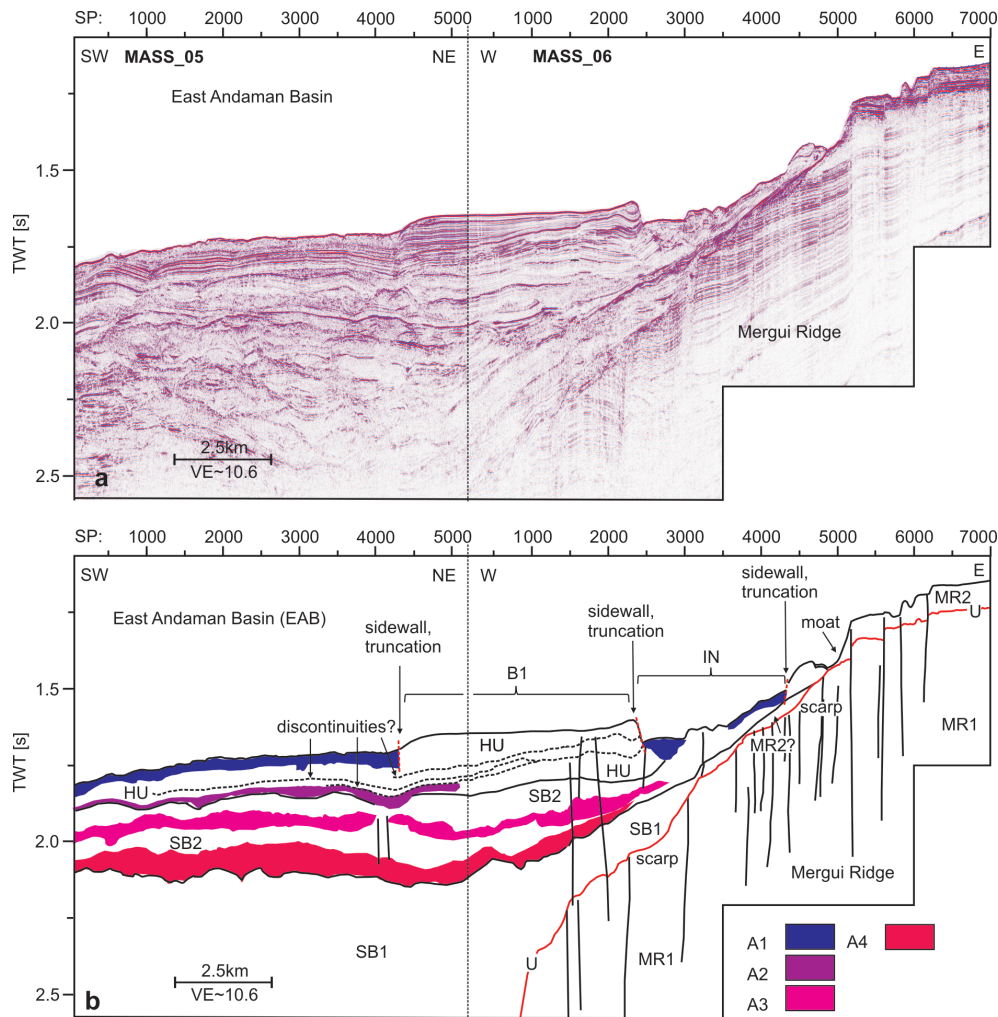
Fig. 5. (a) Seismic profiles MASS_05 and MASS_06, from the southern working area. (b) Interpretation of the profile, showing Mergui Ridge seismic units MR1 and MR2 in the east and basin sedimentary units SB1, SB2 and HU in the SE. The black lines mark boundaries of seismic units. The red line denotes the position of unconformity U. The vertical lines mark the positions of faults. The colored areas denote the position of MTDs within the basin sediments. The black dashed line marks discontinuities within the upper unit HU, indicative of drift deposits. B1 marks a stable block/slide margin, confined by steep sidewalls, and bordered by disturbed sediment bodies of superficial deposit MTD A1; "IN" indicates an incision in the sedimentary column. See Figs. 2 and 3 for the location of the profiles and text for further explanations.

environment at the western edge of Mergui Ridge. In this area, individual blocks have been displaced and faults are cutting through the surface. A smaller block is situated basinward of these deformed MR1 sediments. A pronounced erosive unconformity (U) bounds unit MR1 at its top. The unconformity is traceable on top of the Mergui Ridge (Figs. 4–7). In the southern working area, unconformity U can be traced westward into the East Andaman Basin (Figs. 4 and 5). To the north, where MR1 exhibits a more transparent/chaotic reflection pattern in its upper part, unconformity U is difficult to trace to the East Andaman Basin (Figs. 6 and 7). We interpret the chaotic reflection pattern of the upper part or MR1 as depositions of slope channels as such channels are visible in the bathymetric data of this area (Fig. 3). However, these depositions do not extent across the edge of Mergui Ridge. In addition, large-scale buried slope parallel channel incisions, reaching incision depths of up to ca. 200 m are identified in places within MR1 (Figs. 6 and 7). Such slope-parallel channels are identifiable from the bathymetry as well (Fig. 3).

Seismic unit MR2 is overlying the acoustic basement and unit MR1 on top of Mergui Ridge with a maximum thickness of around 100 m (Fig. 4). In places, it has an eroded irregular top with truncated reflectors (Fig. 5). This indicates an erosive phase between deposition of MR2 and the unit on top. MR2 is exposed to the seafloor at the edge of Mergui Ridge, forming an irregular topography (Figs. 5 and 6). Downslope of the edge of Mergui Ridge, eroded packages of MR2 seem
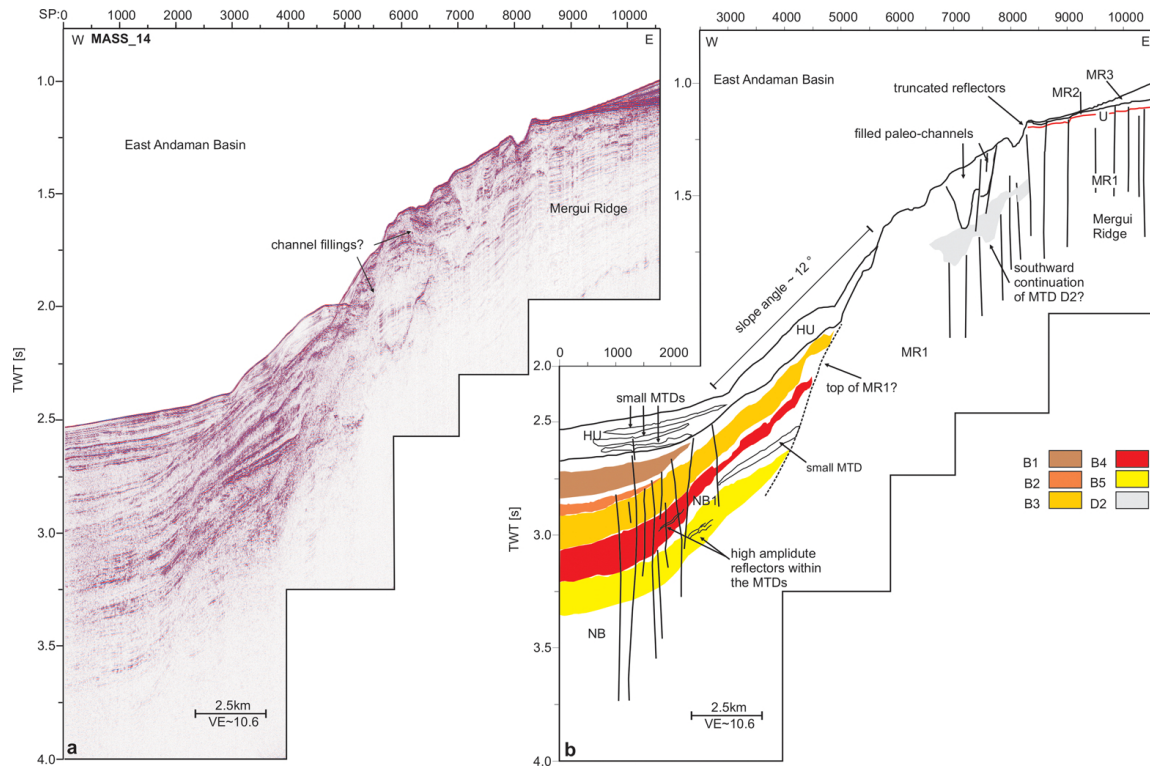
Fig. 6. (a) Seismic profile MASS_14, running across the basin-ridge transition in the northern working area, with channel-fillings indicated at the edge of Mergui Ridge. **(b)** Interpreted profile showing Mergui Ridge units MR1–MR3 in the east and basin sediments NB and HU in the west. The black lines mark boundaries between the seismic units. The red line denotes the position of unconformity U. The black stippled line marks the possible upper boundary of MR1. Channel fillings are present in the upper part of MR1. The reflectors of the upper Mergui Ridge units (MR2 and MR3) are truncated at the edge of the ridge. At the edge of the ridge a U-shaped structure is present, indicating an approximate slope parallel paleo-channel. The coloured areas mark the position of the stacked MTDs B1–B5 and a possible southward continuation of MTD D2. See text for further explanations and Figs. 2 and 3 for location of the profile.

to be present partially on top of the basinward continuation of unconformity U (Fig. 4).

Seismic unit MR3 is the youngest of the Mergui Ridge units. It is deposited on top of MR2. The thickness of this unit varies between about 120 m and 40 m; it is tapering out towards its seaward edge. Marginal valleys and mounded structures are present at the surface within MTD3 around the morphological highs on top of Mergui Ridge (Fig. 3).

4.1.2 East Andaman Basin South

Directly west of the Mergui Ridge lies the East Andaman Basin, which comprises water depths between 900 m and 2200 m. Sediments, infilling the East Andaman Basin, are resolved in the dataset to a subsurface depth of up to about 900 m. In the southern working area, we differentiate three seismic units within these basin sediments. SB1 is the oldest basin fill unit. It exhibits a disturbed acoustic character with reflectors of varying amplitude and continuity (Fig. 2). Towards its landward termination, the oldest basin fill unit SB1 is directly overlying MR1/MR2 sediments (Figs. 4 and 5).

SB1 is overlain by SB2. SB2 shows packages of well stratified, continuous to sub-continuous parallel reflectors of weak-to-moderate amplitudes, separated by pronounced reflectors of high amplitude (Fig. 2). Towards its upslope edge, SB1 onlaps against MR1/MR2 and it is confined by a moat (Figs. 4 and 5). Sediment waves are a characteristic feature of this up to 300 m thick unit (Fig. 4). Narrow vertical zones of low amplitude, crossing several reflectors, are evident within SB2 (Fig. 8b). These features may represent fluid migration pathways. At one location, a possible bottom simulating reflector (BSR) has been identified at subsurface depths around 80 m (Fig. 4c). The youngest unit HU, deposited on top of SB2, shows very regular, parallel, high-amplitude reflectors, with amplitude strengths increasing towards the seafloor (Fig. 2). Based on its reflector characteristics, it is interpreted as a hemipelagic deposit, which is undisturbed in most parts. Sediment waves have a topographic expression in this unit (Fig. 4). Towards the surface, a few zones with small scale faulting are evident within HU (Fig. 8b).
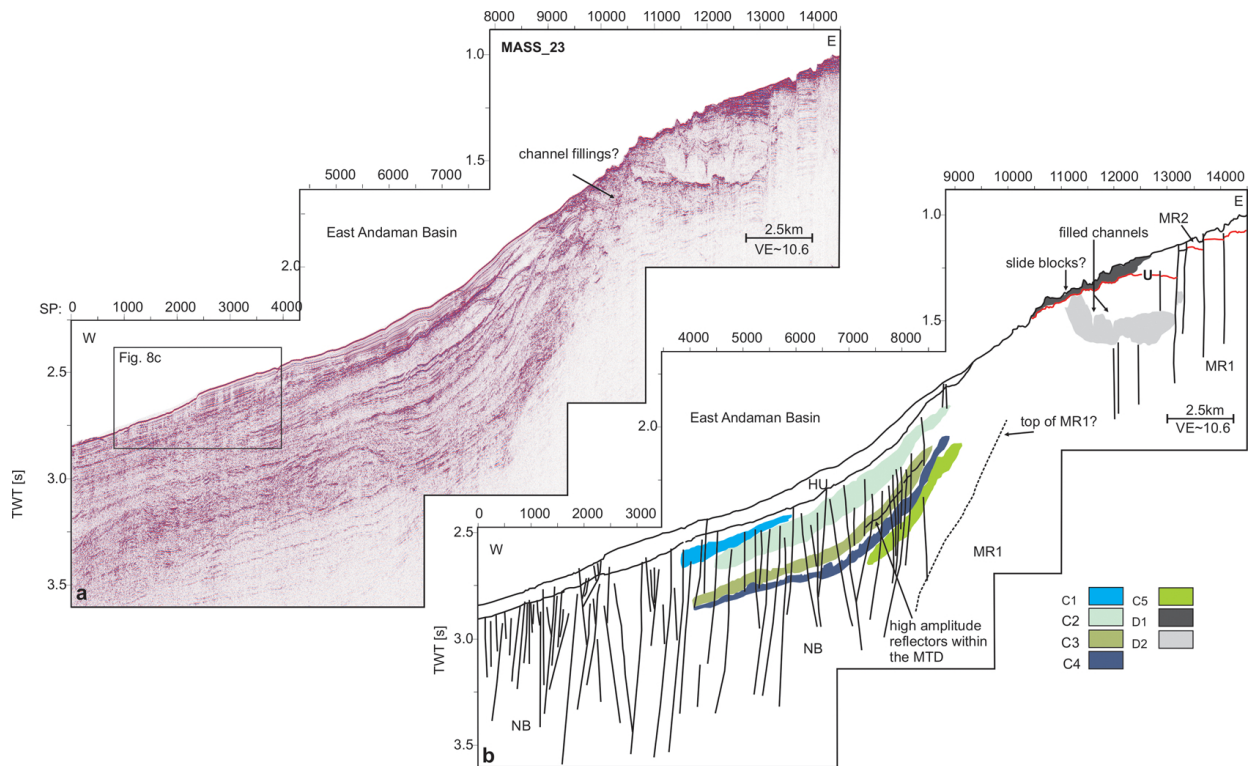
Fig. 7. (a) Slope normal seismic line MASS_23 from the basin ridge transition in the northern working area with channel fillings indicated at the edge of Mergui Ridge **(b)** Interpreted profile, showing seismic units of Mergui Ridge in the east (MR1, MR2) and seismic units of basin sediments in the west (HU, NB). The black lines indicate boundaries between units. The red line marks the position of unconformity U. The black dashed line marks a possible top boundary of MR1 towards the basin. The vertical lines indicate fault positions. The colored areas mark the stacked MTDs C1–C5 in the basin area and MTDs D1 and D2 on Mergui Ridge. See Figs. 2 and 3 for location of profile and text for further explanation.

4.1.3 East Andaman Basin North

We differentiated two seismic units within the northern basin sediments. The lower unit (NB) onlaps the Mergui Ridge unit MR1. Several bodies, characterized by transparent/low amplitude chaotic reflections are alternating with sediments imaged as high-amplitude reflections within NB (Figs. 6 and 7). Deformation of NB sediments is evident from numerous normal faults, dissecting the entire basin fill into blocks and leading to a rather disturbed appearance of NB (Fig. 7).

We did not correlate the lower units in the southern working area (SB1, SB2) and the lower unit in the north (NB). No seismic lines for direct lateral correlation are available. Although these units show similar characteristics, such as high amplitude reflectors alternating with low-amplitude packages, a clear correlation is not possible due to the disturbed character of NB and the lack of an internal boundary within NB, corresponding to the boundary between SB1 and SB2.

The older NB basin sediments in the north are overlain by an up to 200 m-thick hemipelagic unit characterized by parallel and fairly continuous/sub-continuous reflectors. The seismic character of this unit is very similar to the southern unit HU. Hence, we assume that this unit is the same and it is

also labeled as HU (Figs. 6 and 7). HU is quite undisturbed, in contrast to the unit NB below it. However, some faults are cutting through HU to the surface. Along one of these faults, the seafloor is displaced by about 20 m (Fig. 8c). Seaward of this fault, the sediments show a wavy pattern (Fig. 8c). Vertical transparent zones, interpreted as potential fluid migration pathways, are present in the seismic unit HU (Fig. 8c)

4.2 Distribution and dimensions of mass transport deposits

Seventeen individual mass transport deposits (MTDs) were identified in the three different environments described above. Four MTDs are located in the southern basin area (MTD A1–A4), ten MTDs in the northern part (MTD B1–B5 and MTD C1–C5), and three MTDs on Mergui Ridge (MTD D1–D3). The positions of the MTDs, their boundaries and minimum areal extents, as far as they were traceable on the dataset, are illustrated on Fig. 3. The MTDs identified within the basin sediments (A1–A4, B1–B5, C1–C5) are generally characterized as lens- or wedge-shaped bodies, partially with a hummocky surface. They reveal
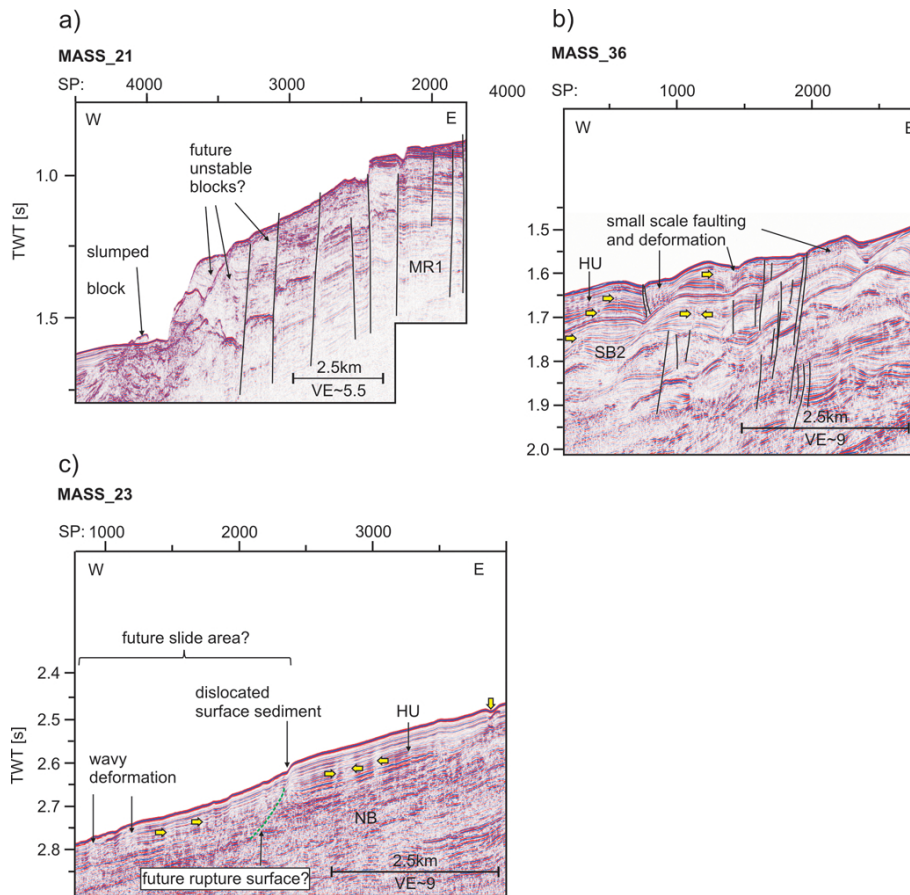
Fig. 8. Possible locations of future slope failures from the Mergui Ridge setting (MASS_23), the East Andaman Basin in the southern working area (MASS_36) and the East Andaman Basin in the northern working area. **(a)** Seismic profile from the edge of Mergui Ridge located slightly south of MTDs D1 and D2. Several faults, marked by black lines, cut to the surface and indicate recent deformation and dislocation of blocks. A small slumped block may indicate that some failure already occured. **(b)** Profile MASS_36 shows drift sediments from the southern working area. Fluid migration pathways are imaged in these sediments as transparent narrow vertical zones (yellow arrows). Small scale faulting and deformation of the upper sedimentary layers may indicate future failure of the drift deposits. **(c)** Seismic profile MASS_23 reveals numerous vertical transparent features interpreted as pathways for fluids (yellow arrows), and a fault dislocating the sea floor (green dotted line), that might act as future rupture surface. Wavy deformation of the surficial sediments downslope of this fault may indicate remobilization of the sediment. See Figs. 2 and 3 for location of profiles, and text for further explanations.

internal chaotic to transparent reflector characteristics (see Fig. 2 for examples of acoustic facies).

4.2.1 MTDs in the southern working area (A1–A4)

Four MTDs have been identified within basin sediments of unit SB2 and HU (A1–A4, Figs. 4 and 5) on the flank of the East Andaman Basin in the southern working area (see Fig. 2 for location). Estimated minimum volumes of these deposits range between $0.3\,km^3$ and $3\,km^3$ (Table 1).

At or close to the seafloor (Figs. 3, 4 and 5) we identified several bodies with disturbed internal structure, interpreted as MTDs. From our dataset we cannot clearly identify if these bodies are interconnected. As they occur in close proximity to each other and in the same stratigraphic depth, we interpreted them to belong to one failure event. There-

fore, we include them all in MTD A1 for the volume estimation. Being situated at or very close to the seafloor, MTD A1 is likely one of the youngest mapped slide deposits. Within the MTD A1, partially sub-parallel reflections are preserved, indicating that movement of slide bodies caused only limited internal deformation (Fig. 4c). Individual bodies/lobes of MTD A1 are found east and southwest of an un-mobilized sediment block (B1 on Fig. 5). This block shows an undisturbed internal structure characteristic for units HU/SB2. It is truncated by steep, about 65 m–high sidewalls. Depending on the motion direction of the slides, B1 may represent a stable in-situ block within the slide area of MTD A1, or the margin of the slide (Fig. 3). Northeast of B1, a 700 m wide and up to 65 m deep incision, marked as IN in Fig. 5, is confined by truncated sidewalls at its eastern and western boundaries, which indicate erosion and removal of sediment.

This structure is interpreted as an evacuated area, which was most likely created during the failure of MTD A1. Disturbed small sediment bodies interpreted to belong to the MTD A1 are located inside the evacuated area. Volumes of MTD A1 deposits are estimated to be $\sim 1.3\,\mathrm{km}^3$, which then is a minimum estimate for MTD A1.

MTD A2, A3 and A4 are buried mass transport deposits (Figs. 4 and 5) within seismic units HU and SB2. They are characterized by transparent to chaotic internal structures and hummocky tops. The boundaries of the individual MTDs are not easily detectable because of the overall low amplitude reflectors of the surrounding background sediment. MTD A4 is the largest slide body identified in the southern working area with an estimated volume of $3.0\,\mathrm{km}^3$ (Figs. 4 and 5, Table 1).

4.2.2 MTDs in the northern working area (B1–B5 and C1–C5)

In the northern working area (see Fig. 2 for location), mass transport deposits were identified in two locations within seismic unit NB (Figs. 3, 6 and 7). In both settings, several stacked MTDs are located at the basin-slope transition (B1–B5 and C1–C5). Figure 3 shows positions and extents of the deposits as mapped out based on the available data set. Figure 2 gives examples of the acoustic characteristics of these bodies.

The seismic profile in Fig. 6 shows at least five stacked slide deposits (B1–B5), originating at or near the slope of Mergui Ridge within background sediments of unit NB. The volumes of the mapped parts of these deposits range from $0.3\,\mathrm{km}^3$ to $3.4\,\mathrm{km}^3$ (Table 1). The mapped slide bodies contain patches of higher amplitude reflections (Fig. 6). These reflections possibly result from un-deformed blocks within the MTDs. An alternative explanation for these higher amplitude reflections may be multiple failure events. The high amplitude reflectors may then represent boundaries between individual events. Several smaller MTDs are present in the vicinity of Mergui Ridge, predominantly in unit HU, but also in the deeper parts of the basin sedimentary succession (Fig. 6).

The MTDs C1–C5 (Fig. 7) are located within the same basin-slope transition setting as MTDs B1–B5 and they are also stacked slide deposits, but their thicknesses are smaller than those of B1–B5 (Table 1). It is also difficult to determine individual slide bodies at this location, because the background sediment in this part of the basin is generally disturbed and exhibits widespread irregular reflector characteristics. Hence, only chaotic to transparent areas without traceable reflectors were mapped as slide bodies. Volumes and depths are listed in Table 1.

4.2.3 MTDs on Mergui Ridge (D1–D3)

Estimated volumes of the MTDs identified in the Mergui Ridge setting (see Fig. 2 for location of setting and Fig. 3

for location of MTDs) range between $0.9\,\mathrm{km}^3$ and $14\,\mathrm{km}^3$ (Table 1). The individual MTDs exhibit very different characteristics in terms of external and internal structures.

MTD D1 consists of displaced sediment blocks with disturbed internal structure (Fig. 9). These blocks are located near the seafloor at the western edge of Mergui Ridge. The high amplitude reflectors inside these blocks show characteristics similar to those of MR2 sediments. This suggests that MTD D1 consists of remobilised MR2 sediment. The partly preserved stratification of the blocks implies that deformation was probably not strong and the blocks have not moved very far. As MTD D1 is situated close to the seafloor, its boundaries are deducible from seafloor morphology. The possible extent of MTD D1 therefore was deduced from the bathymetric dataset (Fig. 3).

MTD D2 is found within seismic unit MR1 (Figs. 7 and 9). Compared to the other MTDs, it shows a large maximum thickness of up to 230 m. The body of MTD D2 comprises blocks ranging from acoustic transparency to some weak internal sub-parallel layering. Its top is eroded (Figs. 7 and 9) and its slide toe is deformed (Fig. 9a). A possible rupture surface is located at the base of MTD D2 (Fig. 9). A steep depression in the seafloor morphology is located upslope of the head area of MTD D2 (Fig. 9b). This 75 m-deep incision is characterized by slope angles of up to 13.5°. The incision can also be identified on the bathymetry, where it shows an amphitheatric shape, typical for a landslide headwall (Fig. 3). The southern boundary of MTD D2 is not very clearly identifiable in the seismic dataset (Fig. 6); the MTD may therefore actually be larger than mapped.

MTD D3 is situated on the flat top of Mergui Ridge, interbedded in the strata of MR3 (Fig. 4). Due to its internal chaotic structure, we categorize it as a MTD, although no headwall or other indicators typical of slide deposits are observed. MTD D3 is traceable over a large part of the working area (about $580\,\mathrm{km}^2$). Despite its large areal extent, it has a maximum thickness of about 60 m. MTD D3 comprises the largest volume of all identified MTDs (about $14\,\mathrm{km}^3$). Erosive structures and channel fills at the top of MTD D3 imply that its original thickness may have been larger. Moreover, its eastward maximum extent may not be covered by our dataset, which also implies a larger original volume of the deposit.

4.3 Recurrence of failure events

Approximate time intervals between individual slide events (A1–A4, B1–B5, C1–C5) have been established for the MTDs in the southern and northern East Andaman Sea settings (see Fig. 3 for locations) following the approach described in Sect. 3. For the southern working area (A1–A4) they range between 940 ka and 1.19 Ma; for the northern working area between 220 ka and 1.47 Ma (B1–B5) and 370 and 950 ka (C1–C5), respectively (Table 2). For the MTDs on Mergui Ridge (D1–D3), no calculation of recurrence intervals have been established as information on sedimentation
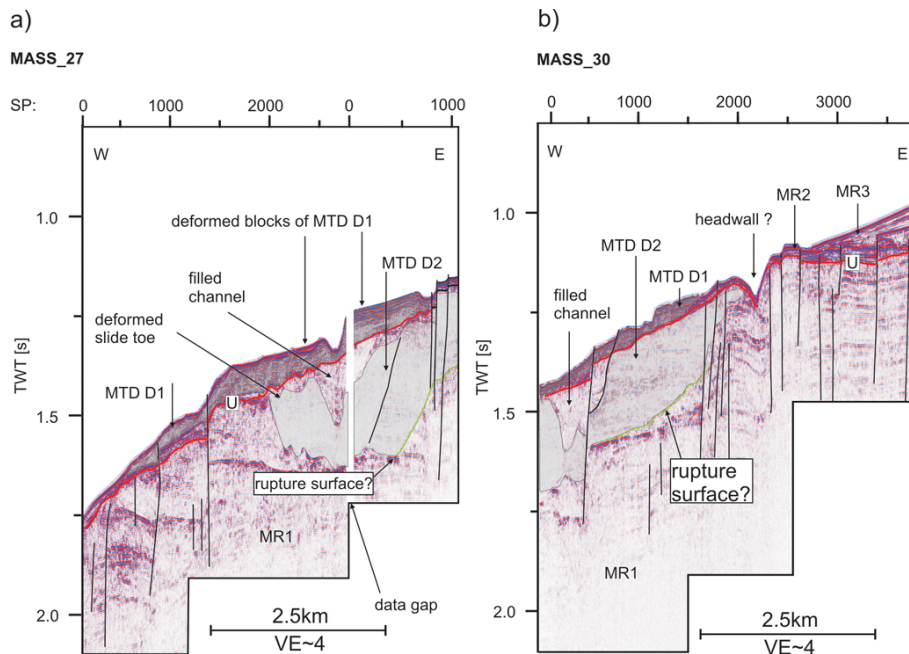
Fig. 9. Seismic profiles showing the edge of Mergui Ridge. The vertical lines indicate positions of faults. The red line marks unconformity *U*. **(a)** Deformed toe of MTD D2 (coloured in light grey). **(b)** Head area of D2 (coloured in light grey) with a steep scarp at its upper part, which may represent the modified head wall (see text for details). The green dotted line indicates the location of a possible rupture surface of D2. See Figs. 2 and 3 for the location of the profiles.

rates was not available. The subsurface depths of the uppermost MTDs in the northern working area range between 100 and 150 m for B1 and between 40 and 120 m for C1.

5 Discussion

5.1 General development and influences on background sedimentary units

5.1.1 Hemipelagic sedimentation

The reflector characteristics of the youngest seismic units HU and MR3 indicate recent hemipelagic sedimentation in the working area (Figs. 4–7). Main sedimentary components in the working area are derived from terrestrial detritus and biogenic production (Keller and Richards, 1967; Rodolfo, 1969; Colin et al., 1999). Regarding sediment type and sedimentation rates, there are differences between the area on top of Mergui Ridge and the downslope basin area of the East Andaman Basin. Whereas on top of the ridge, sediments mainly consist of foraminiferal oozes, silty clays prevail in the adjacent basin area (Keller and Richards, 1967; Rodolfo, 1969). The outer shelf of the Thai-Malay peninsula is described as sediment starved (Rodolfo, 1969; Andreason et al., 1997; Panchang et al., 2008). Rodolfo (1969) described relict foraminifera and relict corals in modern sediments of the Mergui area, implying that sedimentation rates on the Mergui Ridge are generally low and/or mainly related to biogenic

input (Rodolfo, 1969). Left lateral movement along Ranong Fault (Fig. 1) is described as the cause for diversion of river systems towards the Gulf of Thailand and subsequently reduced riverine input from the Thai-Malay Peninsula since the Miocene (Andreason et al., 1997). Recent sediment starvation along the western outer shelf of the Thai-Malay peninsula is explained by Rao et al. (2005) to be due to the trapping of the Ayerawaddy riverine input in the Gulf of Martaban, and direct transfer into the deeper parts of the Andaman Sea by submarine canyons. Detritus delivered by via the Malacca Strait is also deposited only in the deeper parts of the Andaman Sea (Keller and Richards, 1967). Therefore, input of terrigenous material is largely restricted to the areas off the ridge, and sedimentation rates on top of the Mergui Ridge are low, whereas they are moderately high in the off-ridge part of the working area (around $10 \, \text{cm} \, \text{ka}^{-1}$, Rodolfo, 1969, Fig. 1).

5.1.2 Sediments of Mergui Ridge

Comparison of our data set with data from the Mergui Basin (Fig. 1) east of Mergui Ridge (Polachan, 1988) suggests an approximate age of Lower Miocene for unit MR2, a large hiatus between units MR2 and MR3 and a Plio-Pleistocene age of unit MR3. MR1 reveals faulting at the western edge of Mergui Ridge (Fig. 4). Extensive faulting along the western flank of Mergui Ridge is explained by several authors by extension due to basin formation processes all over the Andaman Sea (Polachan et al., 1991; Curray, 2005; Jha et

al., 2010; Kishore et al., 2010; Morley et al., 2011). According to Morley et al. (2011), rifted sequences are deposited at the western flank of Mergui Ridge as a result of this extension. These late syn-rift deposits west of Mergui Ridge were probably deposited during formation of the East Andaman Basin in Late Oligocene/Early Miocene in an open-marine environment (Jha et al., 2010). As the deposition of MR1 clearly predates the Lower Miocene unit MR2, and its reflector characteristics indicate that the sediments are deposited in a hemipelagic environment, we speculate that the sediments of unit MR1 correspond to these synrift sequences and form an older eroded slope of Late Oligocene/Early Miocene age deposited in the marine environment that was prevailing in the area since Early Miocene (Jha et al., 2010). Younger sediments on top of Mergui Ridge (MR2/MR3) are not tectonically deformed.

5.1.3 Drift deposits in the East Andaman Basin and on top of the Mergui Ridge

Jha et al. (2011) described a post-rift sedimentary succession in the region directly west of our working area. They identified a lower sequence containing a chaotic seismic facies interpreted as mass flow complexes, and an upper sequence characterized by pelagic sedimentation since Late Miocene. This upper sequence is described to exhibit mass flow deposits in places and to be influenced by contour currents. Jha et al. (2011) attribute the mass flows within their lower sequence to subsidence in the East Andaman Basin caused by rifting in the Central Andaman Basin since Late Miocene. The presence of mass flows in their upper unit is attributed to disturbances due to modern sea-floor spreading in the Central Andaman Basin since Late Plio-Pleistocene. The sedimentary succession in the southern working area (SB1 and SB2, see Fig. 2 for location) reveals a pattern similar to that described by Jha et al. (2011). Seismic unit SB1, situated on top of the assumed synrift sediments of MR1, reveals largely disturbed sediments, possibly attributable to an older mass flow complex and correlatable to the mass flow unit described by Jha et al. (2011).

The unit SB2 comprises distinct low amplitude packages, separated by high amplitude reflectors. Sediment waves are present (Fig. 4). Rebesco and Stow (2001) described characteristics of elongated plastered drift deposits. Typical features are erosive moats at their boundaries and fields of migrating sediment waves within the deposits. Seismic characteristics of drift deposits comprise uniform low-to medium amplitude patterns (Nielsen et al., 2008). Moreover, discontinuities within drifts, marked by high amplitude reflectors, are common (Faugères et al., 1999). These criteria are met by seismic unit SB2 and we therefore interpret it as bottom current controlled sedimentary unit. SB2 may correlate to the upper, bottom current influenced unit of Jha et al. (2011). The approximate age of SB2 would then be Plio-Pleistocene.

Hérnandez-Molina et al. (2008) give examples of typical geometries of sediments deposits that develop around obstacles when bottom currents rework sediments. Regarding the current direction, a characteristic marginal valley may persist on the stoss side and a depositional tail on the lee side of the obstacle. Such structures have developed around the carbonate platforms in our working area, reworking sediments of unit MR3 (Fig. 3). We therefore conclude that bottom currents may act over a large part of the working area and influence the sediments on Mergui Ridge as well. In this context, the rugged morphology at the edge of the ridge may be attributed to erosive processes induced by bottom currents.

The presence of reversal currents in the Andaman Sea area is explained to be monsoon controlled (Wirtky, 1961). Such wind driven currents can extend to the bottom and induce sediment reworking (Hollister and McCave, 1984; Shanmugan, 2008). Northwest of our working area (Fig. 1b), a stable, monsoon-induced eddy/gyre is described by Varkey et al. (1996). Measurements revealed currents speeds of $12\,\mathrm{m\,s^{-1}}$ at $500\,\mathrm{m}$ and $10\,\mathrm{m\,s^{-1}}$ at $1000\,\mathrm{m}$ water depth (Varkey et al., 1996). In addition, internal waves and tides are able to influence deep-water bottom currents and their deposits (Shanmugan, 2008). Large amplitude internal waves have repeatedly been observed in the working area (Osburne and Burch, 1980; Nielsen et al., 2004b; Vlasenko and Alpers, 2005). They can affect the water column in the working area as deep as several hundred meters below the surface (Osburne and Burch, 1980; Nielsen et al., 2004b). Vlasenko and Alpers (2005) report in depths of up to 241 m interaction of internal waves with the Dreadnought Bank (see Fig. 1b for location). Such internal waves may be able to rework sediment (Pomar et al., 2012).

Although we do not have direct information on bottom currents, we suggest that the two processes described above may induce or influence bottom currents in our working area in the East Andaman Basin. Therefore, we interpret the character of units SB2 and HU in the southern working area and unit MR3 on top of Mergui Ridge as formed by reworking and deposition of currents.

5.1.4 Tectonically deformed sediments in the East Andaman Basin

The EAFZ is a strike slip fault zone west of the Mergui Ridge (Polachan et al., 1988; Polachan and Racey, 1994; Morley et al., 2011). Polachan (1988) reported branches of the EAFZ cutting through our working area (Fig. 3). Recent fault reactivation has been reported from the Mergui Fault north of the working area (Morley et al., 2011). Jintasearanee et al. (2012) interpreted steep NNE–SSW striking scarps in the bathymetry of our working as fault traces exposed at the sea floor. These observations let us infer that tectonic deformation in the working area is ongoing. The East Andaman Basin sediments in the northern working area (see Fig. 2 for location), especially the older deposits of seismic unit NB,

exhibit features of tectonic movement, such as the presence of numerous faults. Although the youngest basin unit HU exhibits an overall undisturbed character, a few faults cut through this unit in the northern working area (Figs. 7b and 8c). This pattern is in agreement with the description of recent deformation due to activity of fault zones near the working area, such as EAFZ and Mergui Fault.

5.2 Causes for slope instability

Causes for slope failures are manifold and may include (i) sedimentary processes, such as sedimentation at very high rates and resulting excess pore pressures, margin oversteepening, and the deposition/formation of weak layers; (ii) the presence of fluids and resulting overpressure; (iii) tectonic processes, such as fault activity and tectonic steepening; and (iv) cyclic loading by earthquakes (Hampton et al., 1996; Canals et al., 2004; Masson et al., 2006; Yamada et al., 2012 and references therein). The factors relevant for the survey area are discussed below.

5.2.1 Influence of sedimentation on slope stability

Slope channels can act as a sediment conduit from the shelf to the deep sea (Stow and Mayall, 2000). Erosion and oversteepening may also cause slope failure within canyons (Arzola et al., 2008). In our data, channels are mainly evident from the northern area and only directly at the edge of the Mergui Ridge (Figs. 3, 6 and 7). As sedimentation rates are low in the Mergui Ridge area and erosion takes place on the edge of Mergui Ridge (see above), we hypothesize that input of sediments by slope channels into the East Andaman basin may result from erosion of older sediments (MR1). The channels, however, seem to be restricted to the edge of the ridge, and no continuation of them has been detected in the basin sediments further downslope. Hence, we consider their influence on basin sedimentation and slope stability as small, but better data coverage of the basin would be needed to be confident about the distribution of canyons and their influences on slope stability. As sediment transport from the Mergui Ridge into the East Andaman Basin seems to be of minor importance and mainly results from erosion of older Mergui Ridge sediments, rapid sediment load and associated oversteepening and/or development of overpressure may play a role only in the deeper parts of the working area, basinward below the edge of Mergui Ridge (MTDs A1–C5). For the destabilization of sediments on top of Mergui Ridge (MTDs D1–D3) other preconditioning factors must be more important.

5.2.2 Tectonic influence: subsidence and fault controlled failures

Tilting of the slope due to subsidence of a margin can act as a preconditioning factor for slope failure (Masson et al., 2010). The Mergui Ridge has undergone subsidence since the onset of rifting in the Central Andaman Basin in Late Miocene

(Kamesh Raju, 2005) due to dextral movement along EAFZ in Late Miocene (Jha et al., 2010) and/or due to thermal contraction (Morley et al., 2011). Jha et al. (2010) described large scale subsidence as a cause for the formation of mass flows west of our working area. These deposits may be correlatable to our seismic unit SB1 (see above). Recent subsidence rates from the shelf area of the Malacca Strait are in the range of 0.25 mm a^{-1} (Lin et al. (2010). This value is relatively small compared to areas with recent extension, for example the Corinth Basin with a subsidence rate of 1 mm a^{-1} (Lykousis et al., 2007). In addition, subsidence rates tend to decrease after termination of rifting (Prosser, 1993). Therefore, subsidence and steepening may still play a role for slope stability but its influence became probably smaller since the onset of rifting that created the large mass flows described by Jha et al. (2010).

The presence of faults has been suggested to act as controlling or preconditioning factor for slope failures (Dillon, 1993; Hampton, 1996; Anasetti et al., 2012). Except for the top unit HU, large parts of the basin fill sediments in the northern working area (unit NB, see Fig. 2 for location) are tectonically deformed. The MTDs C1–C5 and B1–B5 are located in this environment and we consider fault activity as one of the main reasons for slope failures in our working area. Episodic slope failure due to episodic fault activity has been described by Reicherter et al. (2011) to result in slide deposits interbedded in well stratified layers. A similar pattern can be observed for the MTDs in the northern working area (B1–B5 and C1–C5) (Figs. 6 and 7). Moreover, the MTDs B1–B5 seem to occur in stratigraphic depths similar to those of C1–C5. This would imply laterally contemporaneous failures in the northern working area. We therefore suggest that episodic fault activity was important for weakening the sediments along the slope.

Tectonic deformation may also play a role in development of MTDs on top of/at the edge of the Mergui Ridge (D1–D3), where sedimentation rates are low and oversteepening probably is not a preconditioning factor for slope failure. Surficial MTD D1 and buried MTD D2 are both located at the edge of the Mergui Ridge. Tectonic deformation of the top parts of unit MR1 may have caused the development of unstable blocks that were subsequently dislocated. Internal structures of these blocks are still preserved; therefore, run out distances of blocks seem to be small.

In conclusion, weakening of the sediments due to tectonic activity is considered as a main pre-conditioning factor for slope failure, especially at the basin-ridge transition.

5.2.3 Instable drift deposits

Drift deposits are present in the southern working area (see Fig. 2 for location). Laberg and Camerlenghi (2008) show an interrelation between contourite features and slope instabilities: Drifts generally tend to be prone to liquefaction during seismic loading due to good sorting of their particles and

resulting high porosity. High sedimentation rates in drift deposits may result in rapid loading and development of excess pore pressure. The development of excess pore pressure is further facilitated by gas migration, fueled by high organic matter input from productive water masses along continental margins. (Laberg and Camerlenghi, 2008). All these factors increase the susceptibility of drift sediments for failure (Laberg and Camerlenghi, 2008). Migrating fluids can especially cause build-up of excess pore pressure in upper sediment layers, a process which is well known to be capable for destabilizing slope sediments (Vorren et al., 1998; Stigall and Dugan, 2010). Sediments that build drift deposits in the southern working area contain terrigenous material from the Ayeyawady River and/or the Malacca Strait, whereas sediment input from the Mergui Ridge seems unlikely (see above). Off the ridge, sedimentation rates are high (10 cm ka^{-1}, Rodolfo, 1969). An unusually high content of terrestrial organic carbon has been reported for these sediments (Keller and Richards, 1967; Colin et al., 1999; Bird et al., 2008; Ramaswamy et al., 2008,), which may be favorable of formation of gas within the drift deposits. Jintasaeranee et al. (2012) reported gas-charged sediment at the Mergui Ridge slope area from subbottom profiler data (Fig. 3). Several possible gas migration pathways are imaged on our seismic data as vertical zones of acoustic transparency (see Fig. 8). A possible bottom simulating reflector (BSR) was identified in the southern working area (Fig. 4c). Therefore, we consider that build-up of excess pore-pressure due to migrating fluids and instability of drift deposits was an important pre-conditioning factor for the failure events in the southern working area (MTDs A1–A4).

5.2.4 Final trigger mechanism

An important factor for the formation and recurrence of submarine landslides is the presence of a final trigger leading to the failure of potentially unstable sediments (e.g. Masson et al., 2006). Seismic activity is common along the Sunda trench and also within the Andaman Sea (Lay et al., 2005; Ornthammarath et al., 2011; Khan, 2012; NGDC, Global Significant Earthquake Database, 2012). Neotectonic activities have been reported from many structures in the Andaman Sea, such as the modern spreading centre (Kamesh Raju et al., 2004), the Sagaing Fault (Wang et al., 2011), the Andaman Arc (Radhakrishna et al., 2008), or the West Andaman Fault (Kamesh Raju et al., 2007). Ongoing tectonic activity is also documented in our data as faults reaching the surface. Therefore, earthquakes are likely final triggers for slope failures.

In summary, several concurring factors have contributed to past slope failures. We consider migrating fluids, instability of drift sediments and tectonic activity as most important preconditioning factors. Regular earthquakes may act as final trigger for slope failure.

5.3 Recurrence of mass transport deposits

In the East Andaman Basin, several MTDs were detected at different stratigraphic depths at the basin-ridge transition. The stacking of MTDs in the East Andaman Basin sediments implies recurrent slide events. The ages and hence the recurrence rates for the slides in the working area are difficult to estimate. No age data are published; hence, direct age determinations are not possible. The thickness of undisturbed sediments between individual slide events can be used to estimate the recurrence rates of landslides if accumulation rates are known. However, information on accumulation rates in or close to the working area are sparse. The most reliable value is given by Rodolfo (1969), who suggested an average sedimentation rate of 10 cm ka^{-1} for the basin sediments west of Mergui Ridge. Using this accumulation rate and the mapped sediment thickness between individual slide deposits, calculations of recurrence rates result in values around 100 ka. We would like to point out that the estimates for landslide recurrence intervals contain very large error bars. This simple calculation, however, shows that recurrence rates are several 10 000 to 100 000 yr and not 100 to 1000 yr.

The values are similar for the different settings of the basin sediments. Only one slide in the basin area (MTD A1) is found close to or at the seafloor, while all other slides are deeply buried. However, the presence of several MTDs throughout the working area lets us deduce that landslides occurred repeatedly and that the slope area has been generally unstable and prone to failure.

5.4 Estimation of tsunamigenic potential and indicators for failure susceptibility

5.4.1 Past failures and likelihood of tsunamis

Important criteria that control the tsunamigenic potential of a landslide are volume, stiffness/cohesiveness of the slide material, water depth, and initial acceleration of the landslide (Løvholt et al., 2005; Haugen et al., 2005; Grilli and Watts, 2005; Ward, 2001; Greene et al., 2006). We have no knowledge on the initial acceleration and only sparse information on sediment properties, but we can analyse water depths and volumes of the identified MTDs leading to a qualitative assessment of the likelihood of tsunami generation in the past. Generally, the critical water depth for tsunami generation is given as maximum 1000 m, while the minimum volume sufficient to create a tsunami from a submarine landslide is ∼ 2 km^3 (Greene et al., 2006). We would like to point out these values can only be used as guidelines; large landslides in water depths deeper than 1000 m (Tappin et al., 2001) and small landslides (< 2 km^3) in very shallow water (Rahiman et al., 2007) have triggered tsunamis in the past.

The volumes of the MTDs detected in our working area (0.3–14 km^3, Table 1) are small compared to giant landslides on active and passive margins, which may reach volumes

of several hundreds of cubic kilometers (Hühnerbach et al., 2004; Geersen et al., 2011; Krastel et al., 2012).

In the southern working area (see Fig. 2 for location), only one MTD (A4) comprises a volume $> 2\,km^3$ (Table 1), while the others are less than $2\,km^3$. The presence of discontinuities within background unit SB2 indicates erosive events. Such erosive events are common in drift deposits, due to short term changes of boundary conditions (Faugères et al., 1999). This implies that MTDs identified within SB2 may originally have been larger.

All MTDs in the southern area are located at water depths deeper than 1000 m. Subsidence in the working area is ongoing, but rates have been moderate since cessation of rifting, and therefore the water depth at the time of failure was most likely below 1000 m.

The situation is different for superficial MTD A1. Its source area (see depth of evacuated area IN, Fig. 5) is located at water depths around 1000 m. The mapped volume of MTD A1 is smaller than $2\,km^3$ (Table 1). However, the true extent of this MTD is not known and might be larger than $2\,km^3$. Therefore, MTD A1 may fall in the range of tsunamigenic landslides. In the northern working area, four slide deposits with volumes greater than $2\,km^3$ were found, but none of these MTDs shows a volume of more than $3.5\,km^3$ (MTDs B3, B4, C2 and C3, Table 1). As all of these slides are situated in water depths significantly deeper than 1000 m, it seems unlikely that the relatively small MTDs B3, B4, C2 or C3 triggered a tsunami.

On top of Mergui Ridge all detected MTDs (D1, D2 and D3) are located above/near 1000 m water depth, and MTD D2 and MTD D3 comprise volumes $> 2\,km^3$, whereas MTD D1 which is located near the surface, has a volume below $2\,km^3$ and therefore it has probably not been a tsunamigenic landslide.

MTD D2 comprises a volume of $4\,km^3$. Its toe region is deformed. Similar structures have been described by Frey-Martinez et al. (2006) to occur near the frontal ramp of slides that do not leave the scarp area and are frontally confined. A horseshoe incision is located on the landward side of this deposit (Fig. 3b). In contrast to most landslide scarps, this feature is more similar to an incision than a morphological step (Fig. 9b). The landward flank of the incision, however, is significantly higher than the seaward side. Such shapes of landslide scarps are reported from other areas. Krastel et al. (2011) suggest that such scarps were modified by post-failure processes, especially strong bottom currents. This seems plausible, as bottom currents are acting in the working area. Hence, we interpret the incision as headwall of MTD D2. This headwall is the location of slide initiation and located at around 830 m water depth. Therefore, D2 potentially falls in the range of tsunamigenic slides.

MTD D3 shows the largest (mapped) volume of the slides detected in our working area ($14\,km^3$, Table 1). MTD D3 has a somewhat outstanding position among the MTDs on Mergui Ridge. It is located within the tectonically undisturbed

bottom current influenced unit MR3. A possible source area is not evident from our dataset. Although the conditions for slide initiation and evolution cannot be reconstructed, we can infer that this slide definitely falls in the range of tsunamigenic landslides.

5.4.2 Possible locations of future slope failures and their tsunamigenic potential

Three locations of possible future slope failures were identified in our data set. Slightly south of the location of MTD D2 (see Fig. 3 for location), faults cut through the seafloor (Fig. 8a). As fault reactivation and deformation in the region seems plausible, these deformed back rotated blocks may fail in the future. Moreover, a slumped block is located basinward of this deformed area, which may indicate, that some disintegration and failure already occurred. Masson et al. (2006) suggest that thick slide blocks with a steep headwall (rotational slides) might be particularly effective in tsunami generation even without large displacements. Therefore, future slope failures at this location in relatively shallow water depths between 700 m and 1100 m may definitively be tsunamigenic. Regarding MTD D3 that is also located on Mergui Ridge, we cannot reconstruct initiation or evolution of this MTD, as outlined above. However, we can infer that a potential future failure of the same dimensions at the same water depths of about 500–700 m definitely falls in the range of tsunamigenic landslides.

An area in water depths near 1000 m close to MTD A1 in the southern working area may be prone to future failures (Fig. 8b). Widespread sediment waves in combination with small scale faulting and indications for fluid migration pathways suggest a potentially unstable slope. Jintasaeranee et al. (2012) described numerous small scale failures in this area. Therefore, we conclude that future failures in this area are likely. A failure of significant volume of this part of the slope may be tsunamigenic. However, the area comprises large structural complexity and ongoing tectonic activity. Slope failures from areas with regular seismic activities are expected to be small in size, due to frequent triggers in the form of earthquakes, subsequently, not leaving sufficient time to accumulate large amounts of material for voluminous slides (Völker et al., 2009). Therefore, we would rather expect several small failures of individual sediment packages instead of voluminous failures. Hence, we consider the tsunami hazard emerging from this area as low.

Figure 8c shows an enlargement of the topmost sediment layers of profile MASS_23 in the northern working area. A listric fault cuts and dislocates parts of the superficial sediment of unit HU. This fault may be interpreted as possible future failure surface. Downslope of the surface expression of the fault, the sediment is deformed and destabilization may be indicated by the wavy deformation patterns visible on the seismic data. Migrating fluids may further contribute to future slope instability. However, within the northern working

area, all MTDs as well as the area of potential future slope failure are situated well below 1000 m water depth. Consequently, future slides in the northern part of the East Andaman Basin area may occur but probably do not pose a tsunami hazard.

In summary, the same settings that induced slope failures in the past may also lead to slope failure in the future, but only a few slides show volume and depth values typical for tsunamigenic slides. However, it has to be taken into account that our volume estimations are minimum values, as the lateral boundaries of the MTDs in most cases are not covered by the seismic dataset. Moreover, we cannot exclude a correlation between the stacked MTDs (B1–B5 and C1–C5) in the northern working area, as the settings where they occur show great similarity regarding characteristics, amount and architecture of the MTDs. This implies that more slides than outlined above may have triggered tsunamis in the past. However, even then their number would be small as suggested by the time intervals between the slides.

5.5   Recurrence of landslide tsunamis compared to earthquake tsunamis in the Andaman Sea

The Mergui Ridge–East Andaman Basin transition seems to be unstable and slides seem to occur repeatedly. Most of the identified slides are relatively small ($\sim 2 \, km^3$) and occur at relatively large water depths ($> 1000 \, m$); hence, it is unlikely that these slides triggered significant tsunamis. Though numerous slides were found throughout the working area, their recurrence rate is definitely very long, exceeding 100 ka.

The recurrence rates of major tsunamigenic earthquakes occurring in the Sumatra–Andaman area, which triggered tsunamis also affecting the coast off Thailand, were estimated by Monecke et al. (2008). These authors analysed a 1000-yr sediment record off Northern Sumatra. They identified two older extensive sand sheets with similar sediment characteristics as the sand sheet deposited by the 2004 tsunami and concluded that the 2004 Indian Ocean tsunami is separated from its youngest full predecessor by ~ 600 yr. Similar values for major tsunamis are reported by Jankaew et al. (2008) for the Andaman Sea coast in Thailand suggesting recurrence rates of major earthquake tsunamis in the range of 400–600 yr for the Thai coast. Our estimations of time intervals between individual MTDs suggest that they are in the hundred ka to Ma range and only four potential tsunamigenic landslides were identified in the sedimentary record. Hence, the risk of submarine landslide tsunamis is negligible compared to earthquake-generated tsunamis. Landslide-triggered tsunamis, however, would hit the coast with almost no warning time.

6   Conclusions

We investigated the top and the western slope of Mergui Ridge and the Andaman Basin and found that older background sediments in the working area show clear indications for tectonic deformation and rifting processes, leading to extension and faulting. Younger sediments in the East Andaman Basin and on top of Mergui Ridge are mainly shaped by bottom currents.

Special attention was drawn to the occurrence of MTDs and the related tsunami hazard. Several MTDs as well as potential future slope failure locations were identified within sediments of the Mergui Ridge and East Andaman Basin. Generally, the slope area seems to be unstable and landslides occur repeatedly, mainly because of occurrence of potentially unstable drift sediments, the presence of fluids, and ongoing tectonic activity that produces deformation and generates earthquakes that are most likely the final trigger for the destabilization of the sediments.

Tsunami generation in the past by most of these slope failures is unlikely due to their relatively small size and their occurrence at large water depths. Recurrence rate of (tsunamigenic) landslides is small compared to the frequency of tsunamigenic earthquakes in the area. Hence, we consider the risk of landslide-generated tsunamis for the Thai west coast as very low. Triggering of tsunamis by submarine landslides, however, cannot be excluded, especially for slope instabilities at the edge of or on top of Mergui Ridge, and such a tsunami would hit the Thai coast almost without warning time.

Edited by: K. Schwarzer
Reviewed by: A. Georgiopoulou and one anonymous referee

References

Anasetti, A., Winkelmann, D., Krastel, S., Bialas, J., and Brückmann, W.: The BGR slide off Costa Rica: Preconditioning factors, trigger, and slide dynamics, in: Submarine mass movements and their consequences, edited by: Yamada, Y., Kawamura, K., Ikehara, K., Ogawa, Y., Urgeles, R., Mosher, D., Chaytor, J., and Strasser, M., Advances in natural and technological hazards research, Springer, Netherlands, 289–299, 2012.

Andreason, W. M., Mudford, B., and Onge, E. S. J.: Geologic evolution and petroleum system of the Thailand Andaman Sea basins, in: Indonesian Petroleum Association Proceedings of the Petroleum System of SE Asia and Australasia Conference, May 1997, 337–350, 1997.

Arzola, R. G., Wynn, R. B., Lastras, G., Masson, D. G., and Weaver, P. P. E.: Sedimentary features and processes in the Nazaré and Setúbal submarine canyons, west Iberian margin, Mar. Geol., 250, 64–88, doi:10.1016/j.margeo.2007.12.006, 2008.

Becker, J. J., Sandwell, D. T., Smith, W. H. F., Braud, J., Binder, B., Depner, J., Fabre, D., Factor, J., Ingalls, S.,Kim, S-H., Ladner, R., Marks, K., Nelson, S., Pharaoh, A., Trimmer, R., Von Rosenberg, J., Wallace, G., and Weatherall,P.: Global Bathymetry and Elevation Data at 30 Arc Seconds Resolution: SRTM30_PLUS, Mar. Geod., 32, 4, 355–371, doi:10.1080/01490410903297766, 2009.

Bird, M. I., Robinson, R. A. J., Win Oo, N., Maung Aye, M., Lu, X. X., Higgitt, D. L., Swe, A., Tun, T., Lhaing Win, S., Sandar Aye, K., Mi Mi Win, K., and Hoey, T. B.: A preliminary estimate of organic carbon transport by the Ayeyarwady (Irrawaddy) and Thanlwin (Salween) rivers of Myanmar, Quaternary Int., 186, 113–122, doi:10.1016/j.quaint.2007.08.003, 2008.

Biscontin, G., Pestana, J. M., and Nadim, F.: Seismic triggering of submarine slides in soft cohesive soil deposits, Mar. Geol., 203, 341–354, doi:10.1016/s0025-3227(03)00314-1, 2004.

Blewitt, G., Kreemer, C., Hammond, W. C., Plag, H.-P., Stein, S., and Okal, E.: Rapid determination of earthquake magnitude using GPS for tsunami warning systems, Geophys. Res. Lett., 33, L11309, doi:10.1029/2006gl026145, 2006.

Bondevik, S., Svendsen, J. I., and Mangerud, J.: Tsunami sedimentary facies deposited by the Storegga tsunami in shallow marine basins and coastal lakes, western Norway, Sedimentology, 44, 1115–1131, doi:10.1046/j.1365-3091.1997.d01-63.x, 1997.

Bondevik, S., Mangerud, J., Dawson, S., Dawson, A. G., and Lohne, O.: Record-breaking height for 8000-year-old tsunami in the North Atlantic, EOS, Transactions American Geophysical Union, 84, 289–293, 2003.

Bondevik, S., Løvholt, F., Harbitz, C., Mangerud, J., Dawson, A., and Inge Svendsen, J.: The Storegga slide tsunami–comparing field observations with numerical simulations, Mar. Petrol. Geol., 22, 195–208, 2005.

Brune, S., Babeyko, A. Y., and Sobolev, S. V.: Are tilt measurements useful in detecting tsunamigenic submarine landslides?, Geochem. Geophy. Geosy., 10, Q06002, doi:10.1029/2009gc002491, 2009.

Brune, S., Babeyko, A., Gaedicke, C., and Ladage, S.: Hazard assessment of underwater landslide-generated tsunamis: A case study in the Padang region, Indonesia, Nat. Hazards, 53, 205–218, doi:10.1007/s11069-009-9424-x, 2010.

Buranapratheraprat, A., Laongmanee, P., Sukramongkol, N., Prommas, R., Promjinda, S., and Yanagi, T.: Upwelling induced by meso-scale cyclonic eddies in the Andaman Sea, Coast. Mar. Sci., 34, 68–73, 2010.

Canals, M., Lastras, G., Urgeles, R., Casamor, J. L., Mienert, J., Cattaneo, A., De Batist, M., Haflidason, H., Imbo, Y., Laberg, J. S., Locat, J., Long, D., Longva, O., Masson, D. G., Sultan, N., Trincardi, F., and Bryn, P.: Slope failure dynamics and impacts from seafloor and shallow sub-seafloor geophysical data: Case studies from the COSTA project, Mar. Geol., 213, 9–72, 2004.

Chakraborty, P. P. and Khan, P. K.: Cenozoic geodynamic evolution of the Andaman–Sumatra subduction margin: Current understanding, Isl. Arc, 18, 184–200, doi:10.1111/j.1440-1738.2008.00643.x, 2009.

Colin, C., Turpin, L., Bertaux, J., Desprairies, A., and Kissel, C.: Erosional history of the Himalayan and Burman ranges during the last two glacial-interglacial cycles, Earth Planet. Sc. Lett., 171, 647–660, 1999.

Curray, J. R.: Tectonics and history of the Andaman Sea region, J. Asian Earth Sci., 25, 187–232, 2005.

Dawson, A. G., Long, D., and Smith, D. E.: The Storegga slides: Evidence from eastern Scotland for a possible tsunami, Mar. Geol., 82, 271–276, 1988.

Dillon, W. P., Risch, J. S., Scanlon, K. M., Valentine, P. C., and Huggett, Q. J.: Ancient crustal fractures control the location and size of collapsed blocks at the Blake escarpment, east of Florida, in: Submarine landslides: Selected Studies in the U.S. Exclusive Economic Zone, edited by: Schwab, W. C., Lee, H. J., and Twichell, D. C., US Geological Survey Bulletin, 54–59, 1993.

Doust, H. and Noble, R. A.: Petroleum systems of Indonesia, Mar. Petrol. Geol., 25, 103–129, doi:10.1016/j.marpetgeo.2007.05.007, 2008.

Doust, H. and Sumner, H. S.: Petroleum systems in rift basins – a collective approach in southeast Asian basins, Petrol. Geosci., 13, 127–144, doi:10.1144/1354-079307-746, 2007.

Dutta, K., Bhushan, R., and Somayajulu, B. L. K.: Rapid vertical mixing rates in deep waters of the Andaman Basin, Sci. Total Environ., 384, 401–408, doi:10.1016/j.scitotenv.2007.04.041, 2007.

Faugères, J.-C., Stow, D. A. V., Imbert, P., and Viana, A.: Seismic features diagnostic of contourite drifts, Mar. Geol., 162, 1–38, doi:10.1016/s0025-3227(99)00068-7, 1999.

Fine, I. V., Rabinovich, A. B., Bornhold, B. D., Thomson, R. E., and Kulikov, E. A.: The Grand Banks landslide-generated tsunami of November 18, 1929: Preliminary analysis and numerical modeling, Mar. Geol., 215, 45–57, 2005.

Frey-Martínez, J., Cartwright, J., and James, D.: Frontally confined versus frontally emergent submarine landslides: A 3D seismic characterisation, Mar. Petrol. Geol., 23, 585–604, doi:10.1016/j.marpetgeo.2006.04.002, 2006.

Fujino, S., Naruse, H., Matsumoto, D., Jarupongsakul, T., Sphawajruksakul, A., and Sakakura, N.: Stratigraphic evidence for pre-2004 tsunamis in southwestern Thailand, Mar. Geol., 262, 25–28, 2009.

GEBCO 2008: General Bathymetric Chart of the Oceans (GEBCO), available at: http://www.bodc.ac.uk/data/onlinedelivery/gebco/, last access: 28 June 2012.

Geersen, J., Völker, D., Behrmann, J. H., Reichert, C., and Krastel, S.: Pleistocene giant slope failures offshore Arauco peninsula, southern Chile, J. Geol. Soc. London, 168, 1237–1248, doi:10.1144/0016-76492011-027, 2011.

Greene, H. G., Murai, L. Y., Watts, P., Maher, N. A., Fisher, M. A., Paull, C. E., and Eichhubl, P.: Submarine landslides in the Santa Barbara Channel as potential tsunami sources, Nat. Hazards Earth Syst. Sci., 6, 63–88, doi:10.5194/nhess-6-63-2006, 2006.

Grilli, S. T. and Watts, P.: Tsunami generation by submarine mass failure, I: Modeling, experimental validation, and sensitivity analyses, J. Waterw. Port C.-ASCE, 131, 283–297, 2005.

Grilli, S. T., Taylor, O.-D. S., Baxter, C. D. P., and Maretzki, S.: A probabilistic approach for determining submarine landslide tsunami hazard along the upper east coast of the United States, Mar. Geol., 264, 74–97, 2009.

Hall, R. and Morley, C. K.: Sundaland basins, in: Continent-Ocean Interactions within the East Asian Marginal Seas, edited by: Clift, P., Wang, P., Kuhnt, W., and Hayes, D., American Geophysical Union, Geophysical Monograph, 149, Washington DC, 55–85, 2004.

Hampton, M. A., Lee, H. J., and Locat, J.: Submarine landslides, Rev. Geophys., 34, 33–59, doi:10.1029/95rg03287, 1996.

Harbitz, C. B., Lovholt, F., Pedersen, G., and Masson, D. G.: Mechanisms of tsunami generation by submarine landslides: A short review, Norw. J. Geol., 86, 255–264, 2006.

Hasegawa, H. S. and Kanamori, H.: Source mechanism of the magnitude 7.2 Grand Banks earthquake of November 1929: Double couple or submarine landslide?, B. Seismol. Soc. Am., 77, 1984–2004, 1987.

Haugen, K. B., Løvholt, F., and Harbitz, C. B.: Fundamental mechanisms for tsunami generation by submarine mass flows in idealised geometries, Mar. Petrol. Geol., 22, 209–217, 2005.

Hernández-Molina, F. J., Maldonado, A., and Stow, D. A. V.: Abyssal plain contourites, in: Contourites, Developments in Sedimentology, edited by: Rebesco, M. and Camerlenghi, A., Elsevier, Amsterdam, Netherlands, 345–378, 2008.

Hollister, C. D. and McCave, I. N.: Sedimentation under deep-sea storms, Nature, 309, 220–225, 1984.

Hühnerbach, V. and Masson, D. G.: Landslides in the North Atlantic and its adjacent seas: An analysis of their morphology, setting and behaviour, Mar. Geol., 213, 343–362, doi:10.1016/j.margeo.2004.10.013, 2004.

Hyder, P., Jeans, D. R. G., Cauquil, E., and Nerzic, R.: Observations and predictability of internal solitons in the northern Andaman Sea, Appl. Ocean Res., 27, 1–11, doi:10.1016/j.apor.2005.07.001, 2005.

Jankaew, K., Atwater, B. F., Sawai, Y., Choowong, M., Charoentitirat, T., Martin, M. E., and Prendergast, A.: Medieval forewarning of the 2004 Indian Ocean tsunami in Thailand, Nature, 455, 1228–1231, 2008.

Jansen, E., Befring, S., Bugge, T., Eidvin, T., Holtedahl, H., and Sejrup, H. P.: Large submarine slides on the norwegian continental margin: Sediments, transport and timing, Mar. Geol., 78, 77–107, doi:10.1016/0025-3227(87)90069-7, 1987.

Jha, P., Ros, D., degli Alessandrini, A., and Kishore, M.: Speculative petroleum system and play model of East Andaman Basin from regional geology and basin evolution concepts: Addressing the exploration challenges of an extreme frontier area, 8th Biennial International Conference and Exposition on Petroleum Geophysics, Hyderabad, India, P-261, 2010.

Jha, P., Ros, D., and Kishore, M.: Seismic and sequence stratigraphic framework and depositional architecture of shallow and deepwater postrift sediments in East Andaman Basin: An overview, GeoIndia 2011, Greater Noida, New Dheli, India, 12–14 January, 2011.

Jintasaeranee, P., Weinrebe, W., Klaucke, I., Snidvongs, A., and Flueh, E. R.: Morphology of the Andaman outer shelf and upper slope of the Thai exclusive economic zone, J. Asian Earth Sci., 46, 78–85, doi:10.1016/j.jseaes.2011.11.003, 2012.

Kamesh Raju, K. A.: Three-phase tectonic evolution of the Andaman Backarc Basin, Curr. Sci. India, 89, 1932–1937, http://drs.nio.org/drs/handle/2264/339, 2005.

Kamesh Raju, K. A., Ramprasad, T., Rao, P. S., Ramalingeswara Rao, B., and Varghese, J.: New insights into the tectonic evolution of the Andaman Basin, northeast Indian Ocean, Earth Planet. Sc. Lett., 221, 145–162, 2004.

Kamesh Raju, K. A., Murty, G. P. S., Amarnath, D., and Kumar, M. L. M.: The West Andaman Fault and its influence on the aftershock pattern of the recent megathrust earthquakes in the Andaman-Sumatra region, Geophys. Res. Lett., 34, L03305, doi:10.1029/2006gl028730, 2007.

Keller, G. H. and Richards, A. F.: Sediments of the Malacca Strait, Southeast Asia, J. Sediment. Res., 37, 102–127, doi:10.1306/74d7166d-2b21-11d7-8648000102c1865d, 1967.

Khan, A.: Seismogenic sources in the bay of bengal vis-à-vis potential for tsunami generation and its impact in the northern bay of bengal coast, Nat. Hazards, 61, 1127–1141, doi:10.1007/s11069-011-9970-x, 2012.

Kishore, M., Jha, P., and Ros, D.: Structural modeling and seismic attributes analysis of synrift sequences in East Andaman Basin: A qualitative approach towards fault seal analysis in a frontier exploration area, 8th Biennial International Conference and Exposition on Petroleum Geophysics, Hyderabad, India, P-262, 2010.

Krastel, S., Wefer, G., Hanebuth, T., Antobreh, A., Freudenthal, T., Preu, B., Schwenk, T., Strasser, M., Violante, R., Winkelmann, D., and M78/3 shipboard scientific party: Sediment dynamics and geohazards off Uruguay and the de la Plata River region (northern Argentina and Uruguay), Geo-Mar. Lett., 31, 271–283, doi:10.1007/s00367-011-0232-4, 2011.

Krastel, S., Wynn, R. B., Georgiopoulou, A., Geersen, J., Henrich, R., Meyer, M., and Schwenk, T.: Large-scale mass wasting on the Northwest African continental margin: Some general implications for mass wasting on passive continental margins, in: Submarine mass movements and their consequences, edited by: Yamada, Y., Kawamura, K., Ikehara, K., Ogawa, Y., Urgeles, R., Mosher, D., Chaytor, J., and Strasser, M., Advances in natural and technological hazards research, Springer, Netherlands, 189–199, 2012.

Kulikov, E. A., Rabinovich, A. B., Thomson, R. E., and Bornhold, B. D.: The landslide tsunami of November 3, 1994, Skagway Harbor, Alaska, J. Geophys. Res., 101, 6609–6615, doi:10.1029/95jc03562, 1996.

Laberg, J. S. and Camerlenghi, A.: The significance of contourites for submarine slope stability, in: Contourites, Developments in sedimentology, edited by: Rebesco, M., and Camerlenghi, A., Elsevier, Amsterdam, Nertherlands, 537–556, 2008.

Lay, T., Kanamori, H., Ammon, C. J., Nettles, M., Ward, S. N., Aster, R. C., Beck, S. L., Bilek, S. L., Brudzinski, M. R., Butler, R., DeShon, H. R., Ekström, G., Satake, K., and Sipkin, S.: The great Sumatra-Andaman earthquake of 26 December 2004, Science, 308, 1127–1133, doi:10.1126/science.1112250, 2005.

Lin, Y.-n. N., Sieh, K., and Stock, J.: Submarine landslides along the Malacca Strait-Mergui Basin shelf margin: Insights from sequence-stratigraphic analysis, J. Geophys. Res., 115, B12102, doi:10.1029/2009jb007050, 2010.

Lomax, A., Michelini, A., and Piatanesi, A.: An energy-duration procedure for rapid determination of earthquake magnitude and tsunamigenic potential, Geophys. J. Int., 170, 1195–1209, doi:10.1111/j.1365-246X.2007.03469.x, 2007.

Løvholt, F., Harbitz, C. B., and Haugen, K. B.: A parametric study of tsunamis generated by submarine slides in the Ormen Lange/Storegga area off western Norway, Mar. Petrol. Geol., 22, 219–231, doi:10.1016/j.marpetgeo.2004.10.017, 2005.

Lykousis, V., Sakellariou, D., Moretti, I., and Kaberi, H.: Late Quaternary basin evolution of the Gulf of Corinth: Sequence stratigraphy, sedimentation, fault–slip and subsidence rates, Tectonophysics, 440, 29–51, doi:10.1016/j.tecto.2006.11.007, 2007.

Masson, D. G., Harbitz, C. B., Wynn, R. B., Pedersen, G., and Lovholt, F.: Submarine landslides: Processes, triggers and hazard prediction, Philos. T. R. Soc. A, 364, 2009–2039, doi:10.1098/rsta.2006.1810, 2006.

Masson, D. G., Wynn, R. B., and Talling, P. J.: Large landslides on passive continental margins: Processes, hypotheses and outstanding questions, in: Submarine mass movements and their consequences, edited by: Mosher, D. C., Moscardelli, L., Baxter, C. D. P., Urgeles, R., Shipp, R. C., Chaytor, J. D., and Lee, H. J., Advances in natural and technological hazards research, Springer, Netherlands, 153–165, 2010.

Matsumoto, T. and Tappin, D. R.: Possible coseismic large-scale landslide off the northern coast of Papua New Guinea in July 1998: Geophysical and geological results from SOS cruises, Pure Appl. Geophys., 160, 1923–1943, 2003.

Michel, G. W., Yu, Y. Q., Zhu, S. Y., Reigber, C., Becker, M., Reinhart, E., Simons, W., Ambrosius, B., Vigny, C., Chamot-Rooke, N., Le Pichon, X., Morgan, P., and Matheussen, S.: Crustal motion and block behaviour in SE-Asia from GPS measurements, Earth Planet. Sc. Lett., 187, 239–244, doi:10.1016/s0012-821x(01)00298-9, 2001.

Monecke, K., Finger, W., Klarer, D., Kongko, W., McAdoo, B. G., Moore, A. L., and Sudrajat, S. U.: A 1,000-year sediment record of tsunami recurrence in northern Sumatra, Nature, 455, 1232–1234, doi:10.1038/nature07374, 2008.

Morley, C. K.: A tectonic model for the Tertiary evolution of strike-slip faults and rift basins in SE Asia, Tectonophysics, 347, 189–215, doi:10.1016/s0040-1951(02)00061-6, 2002.

Morley, C. K., Woganan, N., Sankumarn, N., Hoon, T. B., Alief, A., and Simmons, M.: Late Oligocene-recent stress evolution in rift basins of northern and central Thailand: Implications for escape tectonics, Tectonophysics, 334, 115–150, doi:10.1016/s0040-1951(00)00300-0, 2001.

Morley, C. K., Charusiri, P., and Watkinson, I.: Structural geology of Thailand during the Cenozoic, in: The geology of Thailand, edited by: Barber, A. J. and Ridd, F. D., Geological Society of London, London, United Kingdom, 539–571, 2011.

National Geophysical Data Center/World Data Center (NGDC/WDC), Significant Earthquake Database, Boulder, CO, USA, available at: http://www.ngdc.noaa.gov/nndc/struts/form?t=101650\&s=1\&d=1, last access: 28 June 2012.

National Geophysical Data Center/World Data Center (NGDC/WDC), Global Historical Tsunami Database, Boulder,

CO, USA, available at: http://www.ngdc.noaa.gov/hazard/tsu_db.shtml, last access: 28 June 2012.

Nielsen, C., Chamot-Rooke, N., and Rangin, C.: From partial to full strain partitioning along the Indo-Burmese hyper-oblique subduction, Mar. Geol., 209, 303–327, doi:10.1016/j.margeo.2004.05.001, 2004a.

Nielsen, T. G., Bjørnsen, P. K., Boonruang, P., Fryd, M., Hansen, P. J., Janekarn, V., Limtrakulvong, V., Munk, P., Hansen, O. S., Satapoomin, S., Sawangarreruks, S., Thomsen, H. A., and Østergaard, J. B.: Hydrography, bacteria and protist communities across the continental shelf and shelf slope of the Andaman Sea (NE Indian Ocean), Mar. Ecol. Prog. Ser., 274, 69–86, doi:10.3354/meps274069, 2004b.

Nielsen, T., Knutz, P. C., and Kuijpers, A.: Seismic expression of contourite depositional systems, in: Contourites, Developments in sedimentology, edited by: Rebesco, M. and Camerlenghi, A., Elsevier, Amsterdam, Netherlands, 301–321, 2008.

Okubo, A., Obata, H., Nozaki, Y., Yamamoto, Y., and Minami, H.: 230th in the Andaman Sea: Rapid deep-sea renewal, Geophys. Res. Lett., 31, L22306, doi:10.1029/2004gl020226, 2004.

Ornthammarath, T., Warnitchai, P., Worakanchana, K., Zaman, S., Sigbjörnsson, R., and Lai, C.: Probabilistic seismic hazard assessment for Thailand, B. Earthq. Eng., 9, 367–394, doi:10.1007/s10518-010-9197-3, 2011.

Osborne, A. R. and Burch, T. L.: Internal solitons in the Andaman Sea, Science, 208, 451–460, doi:10.1126/science.208.4443.451, 1980.

Panchang, R., Nigam, R., Raviprasad, G. V., Rajagopalan, G., Ray, D. K., and Hla, U. K. Y.: Relict faunal testimony for sea-level fluctuations off Myanmar (Burma), J. Palaeon. Soc. India, 53, 185–195, 2008.

Piper, D. J. W., Cochonat, P., and Morrison, M. L.: The sequence of events around the epicentre of the 1929 Grand Banks earthquake: Initiation of debris flows and turbidity current inferred from sidescan sonar, Sedimentology, 46, 79–97, 1999.

Polachan, S.: The geological evolution of the Mergui Basin SE Andaman area, Thailand, Ph.D thesis, University of London, London, 218 pp., 1988.

Polachan, S. and Racey, A.: Stratigraphy of the Mergui Basin, Andaman Sea: Implications for petroleum exploration, J. Petrol. Geol., 17, 373–406, doi:10.1111/j.1747-5457.1994.tb00147.x, 1994.

Polachan, S., Pradidtan, S., Tongtaow, C., Janmaha, S., Intarawijitr, K., and Sangsuwan, C.: Development of cenozoic basins in thailand, Mar. Petrol. Geology, 8, 84–97, doi:10.1016/0264-8172(91)90047-5, 1991.

Pomar, L., Morsilli, M., Hallock, P., and Bádenas, B.: Internal waves, an under-explored source of turbulence events in the sedimentary record, Earth-Sci. Rev., 111, 56–81, doi:10.1016/j.earscirev.2011.12.005, 2012.

Prosser, S.: Rift-related linked depositional systems and their seismic expression, Geological Society, London, Special Publications, 71, 35–66, doi:10.1144/gsl.sp.1993.071.01.03, 1993.

Radhakrishna, M., Lasitha, S., and Mukhopadhyay, M.: Seismicity, gravity anomalies and lithospheric structure of the Andaman Arc, NE Indian Ocean, Tectonophysics, 460, 248–262, doi:10.1016/j.tecto.2008.08.021, 2008.

Rahiman, T. I. H., Pettinga, J. R., and Watts, P.: The source mechanism and numerical modelling of the 1953 Suva tsunami,

Fiji, Mar. Geol., 237, 55–70, doi:10.1016/j.margeo.2006.10.036, 2007.

Ramaswamy, V., Rao, P. S., Rao, K. H., Thwin, S., Rao, N. S., and Raiker, V.: Tidal influence on suspended sediment distribution and dispersal in the northern Andaman Sea and Gulf of Martaban, Mar. Geol., 208, 33–42, doi:10.1016/j.margeo.2004.04.019, 2004.

Rao, P. S., Ramaswamy, V., and Thwin, S.: Sediment texture, distribution and transport on the Ayeyarwady continental shelf, Andaman Sea, Mar. Geol., 216, 239–247, doi:10.1016/j.margeo.2005.02.016, 2005.

Rebesco, M. and Stow, D.: Seismic expression of contourites and related deposits: A preface, Mar. Geophys. Res., 22, 303–308, 2001.

Reicherter, K., Hoffmann, N., Lindhorst, K., Krastel, S., Fernández-Steeger, T., Grützner, C., and Wiatr, T.: Active basins and neotectonics: Morphotectonics of the Lake Ohrid Basin (FYROM and Albania), Z. Dtsch Ges. Geowiss., 162, 217–234, 2011.

Robinson, R., Bird, M., Oo, N., Hoey, T., Aye, M., Higgitt, D., Lu, X., Swe, A., Tun, T., and Win, S.: The Irrawaddy river sediment flux to the Indian Ocean: The original nineteenth-century data revisited, J. Geol., 115, 629–640, 2007.

Rodolfo, K. S.: Sediments of the Andaman Basin, northeastern Indian Ocean, Mar. Geol., 7, 371–402, 1969.

Shanmugam, G.: Deep-water bottom currents and their deposits, in: Contourites, Developments in sedimentology, edited by: Rebesco, M., and Camerlenghi, A., Elsevier, Amsterdam, Netherlands, 59–81, 2008.

Sobolev, S. V., Babeyko, A. Y., Wang, R., Hoechner, A., Galas, R., Rothacher, M., Sein, D. V., Schröter, J., Lauterjung, J., and Subarya, C.: Tsunami early warning using GPS-shield arrays, J. Geophys. Res., 112, B08415, doi:10.1029/2006jb004640, 2007.

Socquet, A., Vigny, C., Chamot-Rooke, N., Simons, W., Rangin, C., and Ambrosius, B.: India and Sunda plates motion and deformation along their boundary in Myanmar determined by GPS, J. Geophys. Res., 111, B05406, doi:10.1029/2005jb003877, 2006.

Stigall, J. and Dugan, B.: Overpressure and earthquake initiated slope failure in the Ursa region, northern Gulf of Mexico, J. Geophys. Res., 115, B04101, doi:10.1029/2009jb006848, 2010.

Stow, D. A. V. and Mayall, M.: Deep-water sedimentary systems: New models for the 21st century, Mar. Petrol. Geol., 17, 125–135, 2000.

Tappin, D. R.: Sediment slump likely caused Papua New Guinea tsunami, EOS Transactions American Geophysical Union, 80, 1999.

Tappin, D. R., Watts, P., McMurtry, G. M., Lafoy, Y., and Matsumoto, T.: The Sissano, Papua New Guinea tsunami of July 1998 – offshore evidence on the source mechanism, Mar. Geol., 175, 1–23, 2001.

Varkey, M. J., Murty, V. S. N., and Suryanarayana, A.: Physical oceanography of the Bay of Bengal and Andaman Sea, Oceanography and Marine Biology: An Ann. Rev., 34, 1–70, 1996.

Vlasenko, V. and Alpers, W.: Generation of secondary internal waves by the interaction of an internal solitary wave with an underwater bank, J. Geophys. Res., 110, C02019, doi:10.1029/2004jc002467, 2005.

Vlasenko, V. and Stashchuk, N.: Three-dimensional shoaling of large-amplitude internal waves, J. Geophys. Res., 112, C11018, doi:10.1029/2007jc004107, 2007.

Völker, D., Weinrebe, W., Behrmann, J. H., Bialas, J., and Klaeschen, D.: Mass wasting at the base of the south central Chilean continental margin: The Reloca slide, Adv. Geosci., 22, 155-167, doi:10.5194/adgeo-22-155-2009, 2009.

Vorren, T. O., Laberg, J. S., Blaume, F., Dowdeswell, J. A., Kenyon, N. H., Mienert, J., Rumohr, J. A. N., and Werner, F.: The Norwegian–Greenland sea continental margins: Morphology and late Quaternary sedimentary processes and environment, Quaternary Sci. Rev., 17, 273–302, doi:10.1016/s0277-3791(97)00072-3, 1998.

Wang, Y., Sieh, K., Aung, T., Min, S., Khaing, S. N., and Tun, S. T.: Earthquakes and slip rate of the southern Sagaing Fault: Insights from an offset ancient fort wall, lower Burma (Myanmar), Geophys. J. Int., 185, 49–64, doi:10.1111/j.1365-246X.2010.04918.x, 2011.

Ward, S. N.: Landslide tsunami, J. Geophys. Res.-Sol. Ea., 106, 11201–11215, 2001.

Weiss, R., Fritz, H. M., and Wünnemann, K.: Hybrid modeling of the mega-tsunami runup in Lituya Bay after half a century, Geophys. Res. Lett., 36, L09602, doi:10.1029/2009gl037814, 2009.

Wyrtki, K.: Physical oceanography of the southeast Asian waters, NAGA Report, Volume 2, Scientific Results of Marine Investigations of the South China Sea and the Gulf of Thailand 1959–1961,The University of California, Scripps Institution of Oceanography, La Jolla, California, 195 pp., 1961.

Yamada, Y., Kawamura, K., Ikehara, K., Ogawa, Y., Urgeles, R., Mosher, D., Chaytor, J., and Strasser, M. (Eds.): Submarine mass movements and their consequences, Advances in natural and technological hazards research, Springer, Dordrecht, Netherlands, 2012.